||| 1.0

4.5
5.0
5.5

||| 2.8 ||| 2.5

||| 3.2 ||| 2.2

||| 3.6

||| 4.0 ||| 2.0

||| 1.1

||| 1.8

||| 1.25 ||| 1.4 ||| 1.6

MICROCOPY RESOLUTION TEST CHART

LEVEL
NAVAL POSTGRADUATE SCHOOL
Monterey, California

THESIS

A COMPUTER STUDY OF THE EFFECT OF ICE
CLOUDS ON THE CEP OF A
ZERO-LIFT REENTRY BODY

by

Martin Warren Mellor

December 1980

Thesis Advisor: A. E. Fuhs

REPORT DOCUMENTATION PAGE		READ INSTRUCTIONS BEFORE COMPLETING FORM
1. REPORT NUMBER	2. GOVT ACCESSION NO. AD-A098 474	3. RECIPIENT'S CATALOG NUMBER
4. TITLE (and Subtitle) A Computer Study of the Effect of Ice Clouds on the CEP of a Zero-Lift Reentry Body		5. TYPE OF REPORT & PERIOD COVERED Master's Thesis; December 1980
		6. PERFORMING ORG. REPORT NUMBER
7. AUTHOR(s) Martin Warren/Mellor		8. CONTRACT OR GRANT NUMBER(s)
9. PERFORMING ORGANIZATION NAME AND ADDRESS Naval Postgraduate School Monterey, California 93940		10. PROGRAM ELEMENT, PROJECT, TASK AREA & WORK UNIT NUMBERS
11. CONTROLLING OFFICE NAME AND ADDRESS Naval Postgraduate School Monterey, California 93940		12. REPORT DATE Dec 80
		13. NUMBER OF PAGES 101
14. MONITORING AGENCY NAME & ADDRESS(If different from Controlling Office) Naval Postgraduate School Monterey, California 93940		15. SECURITY CLASS. (of this report) Unclassified
		15a. DECLASSIFICATION/DOWNGRADING SCHEDULE

16. DISTRIBUTION STATEMENT (of this Report)

Approved for public release; distribution unlimited.

17. DISTRIBUTION STATEMENT (of the abstract entered in Block 20, if different from Report)

18. SUPPLEMENTARY NOTES

19. KEY WORDS (Continue on reverse side if necessary and identify by block number)

Reentry	Ablation	Hypersonic Flow
Trajectory	CEP	Hypersonic Reentry
Ice Cloud	Circular Error Probability	Newtonian Flow
Ice Crystals	Nose	[See page 2]
Ice	Nose Shape	

20. ABSTRACT (Continue on reverse side if necessary and identify by block number)

   The reentry trajectory of a bluff zero-lift reentry body was computed using an HP-9845A computer. To obtain the external shape of an ablating reentry body as a function of altitude, coefficients for polynomial equations were determined. At six discrete altitudes, the calculated nose shapes were identical to published information for the nose shapes of a reentry body with silaceous ablation material. Newtonian flow and an exponential atmosphere were assumed throughout

DD FORM 1473 EDITION OF 1 NOV 65 IS OBSOLETE
1 JAN 73
S/N 0102-014-6601 |

Block 19.   KEY WORDS (Continued)

Humidity
Humidity Sensor
Simulation
Reentry simulation
Silaceous Nose
Zero-Lift

Block 20.   ABSTRACT (Continued)

   The computer program was modified to include ablation due
to ice crystal erosion, and the trajectory was recalculated
for a model ice cloud 5,000 feet thick at an altitude of
30,000 feet. A total of four trajectories was computed for
various values of mass loss fraction for erosion due to ice.
The differences in range from the initial trajectory without
ice erosion were one to fifteen feet.

Accession For	
NTIS GRA&I	✓
DTIC TAB	☐
Unannounced	☐
Justification	
By	
Distribution/	
Availability Codes	
	Avail and/or
Dist	Special
A	

A Computer Study of the Effect of Ice
Clouds on the CEP of a Zero-Lift Reentry Body

by

Martin Warren Mellor
Lieutenant Commander, United States Navy
B.S., Purdue University, 1972
M.S., University of Southern California, 1978

Submitted in partial fulfillment of the
requirements for the degree of

MASTER OF SCIENCE IN MECHANICAL ENGINEERING

from the

NAVAL POSTGRADUATE SCHOOL
December 1980

Author   _____

Approved by: _____
                                    Thesis Advisor

           _____
Chairman, Department of Mechanical Engineering

           _____
              Dean of Science and Engineering

3

ABSTRACT

   The reentry trajectory of a bluff zero-lift reentry body
was computed using an HP-9845A computer. To obtain the
external shape of an ablating reentry body as a function of
altitude, coefficients for polynomial equations were deter-
mined. At six discrete altitudes, the calculated nose shapes
were identical to published information for the nose shapes
of a reentry body with silaceous ablation material. Newtonian
flow and an exponential atmosphere were assumed throughout.

   The computer program was modified to include ablation due
to ice crystal erosion, and the trajectory was recalculated
for a model ice cloud 5,000 feet thick at an altitude of
30,000 feet. A total of four trajectories was computed for
various values of mass loss fraction for erosion due to ice.
The differences in range from the initial trajectory without
ice erosion were one to fifteen feet.

TABLE OF CONTENTS

6

LIST OF FIGURES

LIST OF TABLES

LIST OF SYMBOLS

A   area (ft^2)

A   angle between centerline of body and horizontal plane

B   atmospheric density paramater ($1/23500$ ft^{-1})

C_D drag coefficient

C_p pressure coefficient

C_{p_o} stagnation point pressure coefficient

CEP   Circular Error Probability (ft)

D   drag (1bs)

F   force (1bs)

g   acceleration due to gravity (32.2 ft/sec)

h   altitude (ft)

h   enthalpy

M   Mach number

m   mass (slugs)

$\dot{m}$ mass flux (slugs/sec)

P   pressure

q   dynamic pressure

$\dot{q}$ heat flux

R   Universal Gas Constant

R   distance from the center of the earth to the earth's surface (2.09×10^7 ft)

R   radius of the base of the reentry body

r   local radius of the reentry body

r   distance from the center of the earth to the reentry body (ft)

r'	r/R. distance to reentry body/radius of the earth
T	temperature (absolute)
t	time
v	velocity in the x-direction
V_ϕ	initial velocity
V_e	escape velocity
V_θ	velocity in the theta direction
V	velocity
W	weight (lbs)
x	distance in horizontal direction (ft)
$\ddot{x}$	acceleration in the x-direction (ft/sec^2)
y	altitude above the earth's surface (ft)
$\ddot{y}$	acceleration in the y-direction (ft/sec^2)
α	absorptivity of surface ablator
β	ballistic coefficient; $W/C_D A$ (lb/ft^2)
γ	ratio of specific heats
ϵ	ablator surface emissivity
θ	angle measured from apogee to reentry body
μ	Mach angle
ρ	free stream atmospheric density (slug/ft^3)
ρ_o	assumed mean sea level atmospheric density (0.0027 slug/ft^3)
σ	Stefan-Boltzmann Constant
σ	variance
ψ	angle of local nose surface to centerline (degrees)
ω	angular velocity

Subscripts:

C_s solid surface erosion

g   gaseous products

g_s net value of gaseous products

o   initial value

r   mechanical erosion (liquid or solid)

rad   radiative to the environment

s   net surface value

w   wall or ablator surface value

x   in the x-direction

y   in the y-direction

I. INTRODUCTION

A. BACKGROUND

The Naval Surface Weapons Center, White Oak, Maryland, is partially responsible for providing improved sensors for balloon-carried radiosondes which measure atmospheric properties at various altitudes. One item of ongoing research at White Oak, and initially the object of this thesis, is an improved humidity sensor.

An object of contention within the strategic missile community is whether or not water vapor, rain or ice, i.e., atmospheric humidity phenomena, significantly modify the reentry trajectory of hypersonic zero-lift reentry bodies. In order to determine the influence on the reentry trajectory, the ability to measure accurately water vapor, water droplets and ice crystals must exist.

The humidity sensor currently being used on radiosondes is a carbon hygristor element which has poor time response at high altitudes because of the inherent sensing delays in the hygristor element. For temperatures of -40°C, which corresponds to altitudes above about 30,000 feet, the time lag of the sensing element can be of the order of fifteen minutes [Ref. 1]. Therefore, significant errors in humidity versus altitude maps are encountered.

Table 1 is a reprint from Brousaides [Ref. 1] showing the time response of the currently used carbon hygristor. Various

step changes in relative humidity at several fixed temperatures yield the tabulated time responses to achieve 63% or 90% of the step input.

Table 1. Carbon Element Response Lags
(Reproduced from Brousaides [Ref. 1], p. 16)

RH Level % (Initial-Final)	Temp	Change in RH Indication, sec	
		63%	90%
30-50	0°C	0.1	0.5
51-85		0.3	1.4
85-51		0.4	2.2
51-30		0.3	1.6
31-51	-20°C	2.6	14
50-80		2.4	21
79-51		2.6	48
51-31		3.8	47
31-50	-30°C	15	61
50-72		11	104
72-50		9	169
50-31		33	163
31-50	-40°C	86	363
50-66		82	272
65-50		88	578
50-30		260	727

Table 1 shows that, as temperature decreases, that is, as altitude increases, the time response of the element becomes so slow as to make the readings virtually meaningless for any reasonable rate of upward balloon motion. In the case where ice is to be detected, the time lag of the sensing element is particularly critical.

The object of current research on the hygristor element is to determine a heat transfer model of the sensing element so that the delay times can be calculated as a function of temperature. By relating delay time to temperature and

14

temperature to altitude, a more accurate map of humidity versus altitude can be obtained. If an accurate heat transfer model of the hygristor element can be obtained, data processing can be used to yield accurate measurements. Alternatively, an improved sensor can be designed once the exact cause of the delay can be pinpointed.

Even if humidity can be accurately measured, determination of water droplet or ice crystal concentration and size distribution within a cloud is difficult. In other words, even if humidity can be sensed accurately, can this information be related directly to rain or ice? Perhaps a different type of sensor or several sensors might be needed to determine humidity, cloud composition and concentration.

In addition, in order to design a useful sensor, criteria for measurement accuracy are required. The criteria for sensor accuracy are determined by the sensitivity of the reentry trajectory to changes in water vapor, rain and ice concentrations.

Criteria are not available for determining the change in a reentry trajectory as a function of atmospheric water content. Therefore, it became necessary to start at the beginning in order to learn enough about the reentry process to make estimates of how much the reentry trajectory could differ with changes in humidity-related atmospheric conditions. This thesis estimates the change in range due to clouds with ice crystals.

15

Consequently, basic information concerning hypersonic flow about bluff bodies was studied. Equations of motion for reentry bodies were formulated in relation to the current problem. The many factors relating to reentry, such as ablation, convective and radiative heating and the modifications to ablation because of chemical interaction with water were considered.

B. SCOPE

Three separate atmospheric water phenomena affect reentry ablation. The three phenomena are water vapor, rain and ice crystals. Of the three phenomena, reentry through ice clouds is the most destructive. Consequently, this thesis studies the effects of ice clouds.

II. THEORY

A. REENTRY DYNAMICS

1. Trajectory

The trajectory of interest is the ballistic reentry of a zero-lift vehicle typical of reentry bodies used as warheads. A ballistic missile trajectory is typified by near-orbital reentry velocities and a steep initial flight path angle, i.e., greater than five degrees.

All trajectories of reentry bodies pass through three operational phases. The three operational phases are defined as follows:

a. Keplerian phase: The segment of the trajectory where gas dynamic forces are negligible ($\rho = 0$).

b. Intermediate phase: The segment of the trajectory where gas dynamic forces are of comparable magnitude to other terms (gravity) in the equations of motion.

c. Gas-dynamic phase: The segment of the trajectory where aerodynamic forces dominate the equations of motion for reentry.

Of the three phases described above, the gas dynamic phase is the one in which environmental factors, such as clouds or humidity, influence the trajectory. Therefore, the gas dynamic phase is the only portion of the reentry which will be considered.

The analysis of the flight of the reentry body is a
particular application of the general theory of the dynamics
of rigid bodies in three dimensions. The motion of the center
of mass can be separated from the motion of the body about the
center of mass. In this discussion, since a zero-lift body
is hypothesized, the assumption is made that the center-line
of the body always is parallel to the velocity vector.

In addition, the assumption will be made that the
reentry trajectory is planar rather than three-dimensional.
Motion in the third dimension is, of course, possible and
indeed certain for actual reentry bodies due to wind,
precession, Coriolis force and so forth. However, if the
"particle" can be described as one capable of generating drag
only, then motion in only two dimensions is assured. Conse-
quently, the reentry body appears as a point particle of
varying mass subject to the various forces applied by the
reentry environment.

Atmospheric properties, particularly the densities
existing at higher altitudes, are subject to considerable
uncertainty. In order to provide a model of the density
profile of the atmosphere, two assumptions are made:

1. The earth and its atmosphere are spherically
   symmetrical.

2. The atmospheric density varies exponentially
   with altitude.

The first assumption is reasonable for this analysis
since only a small portion of the atmosphere is traversed
for a ballistic entry. The second assumption is based

18

on the simple kinetic theory of an isothermal gas in a
uniform gravitational field. These assumptions lead to the
well-known exponential model for the atmosphere:

$$\rho = \rho_0 e^{-By} \qquad (1)$$

where: ρ = free stream atmospheric density ($slug/ft^3$)

ρ_0 = assumed mean sea level atmospheric density

B = atmospheric density decay parameter (ft^{-1})

y = altitude of vehicle above the surface of
the earth (ft)

B is equal to the mean molecular weight of the earth's
atmosphere times the local acceleration due to gravity
divided by the product of the mean atmospheric temperature
and the universal gas constant. Figure 1 is a reprint from
Loh [Ref. 2] and compares the exponential approximation
with the ARDC (1956) model of the atmosphere.

2. Equations of Motion

The geometry of an IRBM or ICBM trajectory is shown
in Figure 2 [Ref. 3]. Assuming no friction occurs during
the flight, the conservation of energy gives:

$$1/2 \ mV^2 - mgr = 1/2 \ mV_\phi^2 - mgR = constant \qquad (2)$$

Equation (2) provides a unique relationship between
velocity and altitude provided some initial condition
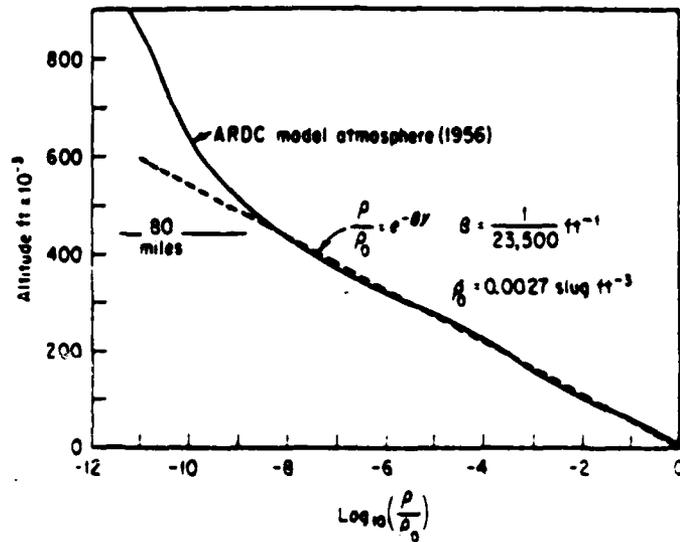
Figure 1.   Comparison of Exponential Approximation
with ARDC Model of Earth's Atmosphere (1956)
(Reproduced from Loh [Ref. 2], p. 13)
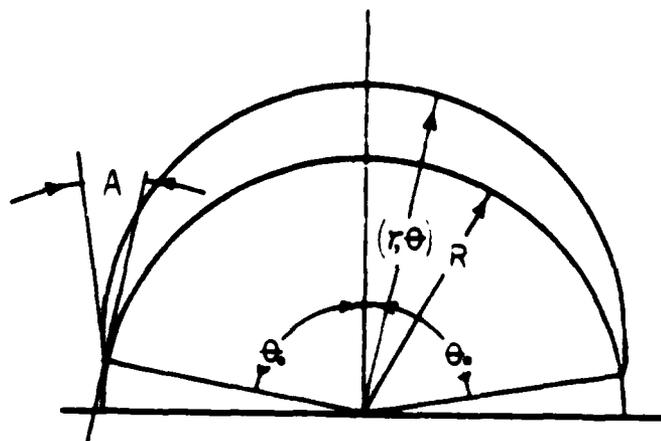
Figure 2.   Diagram of ICBM Flight Path
(Reproduced from Fuhs [Ref. 3])

20

or boundary condition can be used to find the constant term.
Equation (2) also can be written, if $r \approx R$, as:

$$\frac{m}{2}\left[\left(\frac{dr}{dt}\right)^2 + \left(r\,\frac{d\theta}{dt}\right)^2\right] - g\,\frac{R^2 m}{r} = \text{constant} \qquad (3)$$

where the constant in both equations (2) and (3) is the total
reentry energy, i.e., kinetic plus potential energy, of the
body.

The conservation of angular momentum of a constant
mass also applies and can be written as:

$$mr^2 \omega = mr^2\,\frac{d\theta}{dt} = mRV_\theta(0) = mRV_\phi \cos A \qquad (4)$$

Boundary conditions for equations (3) and (4) are $\theta(0) = \theta_0$
and $r(0) = R$. Time can be eliminated from the equations
using the relation from above.

$$\frac{dr}{dt} = \frac{dr}{d\theta}\,\frac{d\theta}{dt} = \frac{dr}{d\theta}\,\frac{RV_\phi \cos A}{r^2} \qquad (5)$$

Substitution of equations (4) and (5) into equation
(3) gives:

$$\frac{dr}{d\theta}\,\frac{RV_\phi \cos A}{r^2} = \sqrt{V_\phi{}^2 - 2gR + \frac{2g\,R^2}{r} - \left(\frac{RV_\phi \cos A}{r}\right)^2} \qquad (6)$$

21

Let

$$Z = [\frac{RV_\phi \cos A}{r} - \frac{gR}{V_\phi \cos A}] \tag{7}$$

Note that

$$dZ = \frac{-RV_\phi \cos A}{r^2} \, dr \tag{8}$$

Substituting equations (7) and (8) into equation (6) yields

$$-\frac{dZ}{d\theta} = \sqrt{V_\phi{}^2 - 2gR + \left(\frac{gR}{V_\phi \cos A}\right)^2 - Z^2} \tag{9}$$

Integrate equation (9) to obtain θ:

$$-\int d\theta = \int \frac{dZ}{\sqrt{V_\phi{}^2 - 2gR + \left(\frac{gR}{V_\phi \cos A}\right)^2 - Z^2}} \tag{10}$$

If

$$\phi^2 = V_\phi{}^2 - 2gR + \left(\frac{gR}{V_\phi \cos A}\right)^2 \tag{11}$$

then equation (10) becomes

22

$$-\int d\theta = \int \frac{dZ}{\sqrt{\phi^2 - Z^2}} = - \arccos \frac{Z}{\phi} + C \tag{12}$$

To evaluate the constant C, symmetry and the boundary conditions $r = R$, $\theta = \pm\theta_0$ and $Z = Z_0$ can be used. Thus:

$$\frac{Z_0}{\phi} = \frac{\cos A - \left(V_\phi \frac{gR}{^2\cos A}\right)}{\sqrt{1 + \left(\frac{gR}{V_\phi^2 \cos A}\right)^2 - \frac{2gR}{V_\phi^2}}} \tag{13}$$

Substitution of the boundary conditions into equation (12) yields:

$$\cos(\theta_0 + C) = \cos(\theta_0 - C) = \frac{Z_0}{\phi} \tag{14}$$

This implies that $C = \pi$ and therefore:

$$\cos(\theta + \pi) = -\cos\theta = \frac{Z}{\phi} \tag{15}$$

At this point, refer to equations (2) and (3), and note that for some value of initial velocity the total energy, i.e., the constant term, will be zero. This value of initial velocity corresponds to the initial velocity at which the

23

particle kinetic energy is equal to potential energy. Since the constant term is zero, as the particle moves, the constant term will remain zero, and kinetic energy will just balance the potential energy for all values of r, even as r approaches infinity. Thus, the value of initial velocity is the escape velocity. Hence

$$V_\phi{}^2 = V_e{}^2 = 2gR \tag{16}$$

Substitute equations (7) and (11) into equation (15) to get

$$\cos\theta = \frac{\dfrac{gR}{V_\phi \cos A} - \dfrac{RV_\phi \cos A}{r}}{\sqrt{V_\phi{}^2 + \left(\dfrac{gR}{V_\phi \cos A}\right)^2 - 2gR}} \tag{17}$$

Define and substitute the relations $V = V_\phi / V_e$ and $r' = r/R$ and equation (16) into equation (17) to arrive finally at

$$\cos\theta = \frac{2 - (2V^2 \cos^2 A)/r'}{(1 + 4V^2 \cos^2 A(V^2 - 1))^{1/2}} \tag{18}$$

Equation (18) is used to calculate a family of curves showing range versus launch angle. In Figure 3, range is

24

found as a function of launch angle be setting $r' = 1.0$ in equation (18) to find θ_o for various values of V between 0.5 and 0.7 and realizing that

$$\text{Range} = 2R\theta_o \qquad (19)$$

where $R = 2.09 \times 10^7$ ft for the radius of the earth.
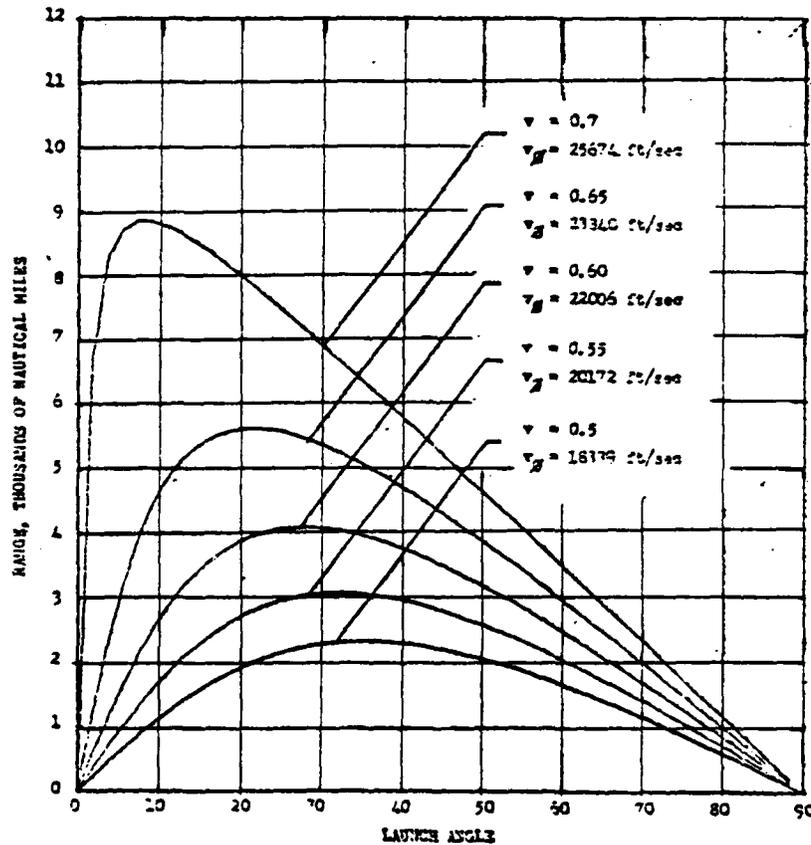
Figure 3.   Range of a Ballistic Missile as a Function of Launch Angle for Various Values of $V = V_\phi/V_e$ (Reproduced from Fuhs [Ref. 3])

A value of V_ϕ can be deduced from Figure 3 by assuming that the missile will be launched with the proper velocity and launch angle to achieve the optimum range, i.e., the peaks of the curves.

For example, Table 2 shows the various characteristics of typical ballistic missiles in the inventory today. The C-4 Trident has a range of between 4000 and 4800 nm. Referring to Figure 4, an optimum range of 4100 nautical miles requires a launch angle of about 27° and V_ϕ of about 22006 ft/sec.

Table 2. Launch Vehicles and Parameters
(Reproduced from Fuhs [Ref. 3])

Missile	Dia Length	Weight	Payload	Range nm	Warhead Yield	IOC	Retired	CEP feet	Stages
A-1 Polaris	54"28'	30,000		1200		Nov 60	Oct 65		2
A-2 Polaris	54"31'			1500					2
A-3 Polaris	54"31'			2500					2
C-3 Poseidon	72"34'		14RV	2300				1800	
C-4 Trident	72"34'	70,000	8MK4	4000 (4800)	100KT	1979?		1500	3
D-4 Trident	82"45.8'			6700					
D-5 Trident	82"45.8'	126,000	14RV 7MK12A		350KT	1985 (1987)			
MX	92"	172,000	14MK12A	6000		1983		(100' due to guidance) (30' gps)	
Atlas							1965		
Titan			MK6						
MMI									
MMII									
MMIII			3MK12A	8000	350KT			600	3

Returning to equation (2), the constant for the C-4
Trident can be found by substituting V_ϕ and R.

$$\frac{1}{2} V_\phi^2 - gR = \frac{\text{constant}}{m} = K \qquad (20)$$

$$K = \frac{1}{2} (22006)^2 - (-32.2)(2.09 \times 10^7) = 9.15 \times 10^8 \ ft^2/sec^2$$

Since K now is known, equation (2) can be used to find the
velocity at any point in the trajectory given r by rewriting
equation (2) as

$$V = [2(K + gr)]^{1/2} \qquad (21)$$

If the portion of the trajectory near reentry is
examined (that is, where r is not much different from R),
the earth can be approximated as being flat since $y/R \ll 1$
where y is altitude. For this case, the simple two-dimensional
equations of motion in Cartesian coordinates apply, that is

$$\Sigma F_x = m\ddot{x} \qquad (22)$$

and

$$\Sigma F_y = m\ddot{y} \qquad (23)$$

where x is distance measured horizontally, and y is distance measured vertically.

Since in the model the only force in the x-direction is drag, and the forces in the y-direction are drag and gravity, equations (22) and (23) can be written as

$$\ddot{x} = - \frac{D_x}{m} \tag{24}$$

$$\ddot{y} = - \frac{D_y}{m} - g \tag{25}$$

where D_x and D_y represent the drag in the x and y directions, respectively. In finite difference form, equations (24) and (25) are

$$\frac{X_{j+2} - 2X_{j+1} + X_j}{\Delta t^2} = - \frac{D_x}{m} \tag{26}$$

$$\frac{Y_{j+2} - 2Y_{j+1} + Y_j}{\Delta t^2} = -g - \frac{D_y}{m} \tag{27}$$

The values of X_1 and Y_1 and $V(0)$ are obtained from initial conditions at the point of interest at the beginning of reentry using equations (18), (19), and (21). The values of X_2 and Y_2 are obtained from

$$X_2 = X_1 + U_o \Delta t \qquad (28)$$

$$Y_2 = Y_1 + V_o \Delta t \qquad (29)$$

where

$$V(0) = \sqrt{U_o^2 + V_o^2} \qquad (30)$$

B. HYPERSONIC REENTRY

The character of the gas dynamic phase of flight at near-orbital velocities is far removed from that of flight at sonic or subsonic velocities. The vehicle has tremendous energy and angular momentum, most of which must be released to the atmosphere. The two processes available to transfer the energy are manifested as heating of the vehicle and deceleration.

No precise definition may be given for the velocity at which supersonic flow becomes hypersonic flow because the effects vary with the vehicle geometry. In addition, the onset of these effects occurs gradually rather than abruptly. Knowledge of Mach number at which transition from supersonic to hypersonic flow occurs is important. If the flow is hypersonic, certain simplifying assumptions can be made concerning the shock shape and position relative to the body, which relate directly to drag and pressure coefficient. These assumptions are discussed below.

During hypersonic flight, there will be regions of the flow fields about a typically blunt-nosed body where the flow decelerates and in which subsonic, transonic and supersonic flows all exist simultaneously. For the purposes of this discussion, a Mach number greater than or equal to four will be considered hypersonic.

Any bluntness of the nose will manifest itself as a detached shock. A pointed nose will melt or ablate due to the intense heat generated at the point and therefore will become blunt. Consequently, the blunted nose generates the detached shock. The most striking effect of hypersonic flight is the formation of a shock ahead of virtually all bodies. The behavior of the shock for the flow past a blunt body of revolution as the Mach number increases may be illustrated as in Figure 4, taken from Cox and Crabtree [Ref. 4], for flow of a perfect gas about a sphere.

As can be seen, the shock stands off from the body at all Mach numbers, and the shock-detachment distance decreases as the Mach number increases. The limiting shock ($M \rightarrow \infty$) lies close to the body and is very nearly concentric over most of the surface of the sphere. Just behind the shock wave where the shock is nearly perpendicular, the flow is brought almost to rest and is subsonic. As the flow passes around the body, the flow accelerates, passes through sonic speed and finally accelerates to supersonic velocities as is illustrated in Figure 5, again taken from Cox and Crabtree [Ref. 4].
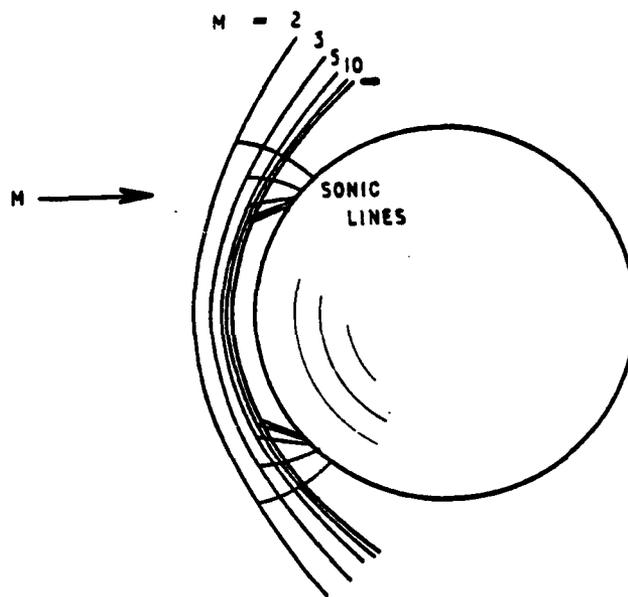
Figure 4. Shock Shapes for Flow Past a Sphere at Different
            Mach Numbers (γ = 1.4). (Reproduced from Cox
            and Crabtree [Ref. 4], p. 9)

At the high temperatures experienced behind the shock in
hypersonic flow, the assumption of a perfect gas cannot be
made as the energies of the gas associated with temperature
are comparable to the energies of various molecular and atomic
processes such as ionization, dissociation and vibration.
Therefore, characteristics of the gas such as the commonly
accepted value of the ratio of specific heats for air, i.e.,
γ = 1.4, must be viewed with skepticism and taken into account
when calculating the flow field.

However, the Mach number can be associated with the ratio
of the kinetic energy and the random thermal energy by the
relation

31

$$M^2 = \frac{(\text{velocity})^2/2}{(\text{speed of sound})^2/2} \simeq \frac{V^2/2}{\gamma RT/2} \propto \frac{\text{kinetic energy}}{\text{thermal energy}} \qquad (31)$$

SHOCK

SONIC
LINE

$M_2 > 1$

$M_2 < 1$

r_s

r_b

$M_1 >> 1$

$M_2 > 1$
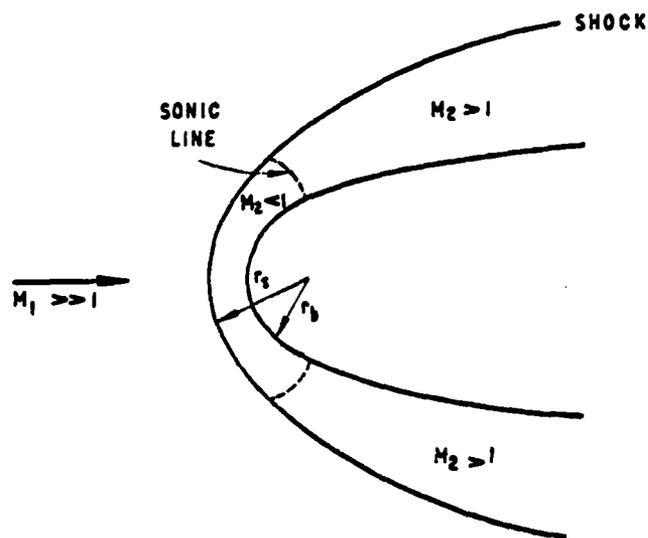
Figure 5. Subsonic and Supersonic Regions for Flow Past a
Blunt Body. (Reproduced from Cox and Crabtree
[Ref. 4], p. 65)

For large Mach numbers, regardless of the value of γ, the
kinetic energy is much larger than the thermal energy. This
implies that the random motion associated with collisions
between atoms and molecules is of relatively little importance
compared to the kinetic energy of the particles and therefore
the gas may be thought of as a stream of non-interacting
particles. The stream of non-interacting particles was first

conceived by Newton for a "rare" gas composed of particles with large distances between them. Newton showed that if the particles do not interact with one another and at large velocities, then the resistance of a body into which the particles collide will vary as the square of the velocity. In addition, he calculated, by assuming that there was no transfer of tangential momentum and that the normal momentum of the particles is destroyed at the surface, that the force on a plate at incidence to the flow varies as the square of the angle of incidence. More recently these assumptions have been used to show that the pressure on the plate is given by

$$\Delta P = \rho V^2 \sin^2 \psi \qquad (32)$$

or

$$C_p = 2\sin^2 \psi \qquad (33)$$

Also, for flow over wedges at high Mach number, the assumptions were used to show that the relation between the shock angle (μ) and the body angle (ψ) is

$$\frac{\mu}{\psi} = \frac{\gamma + 1}{2} \qquad (34)$$

Therefore as $\gamma \to 1$, the body and the shock coincide and the density ratio across the shock becomes infinite. Thus there is a layer of high density gas lying near the surface.

33

This is the "Newtonian Shock Layer" or entropy layer since very large changes in entropy also occur.

Lees [Ref. 5] adjusted the Newtonian Formula [equation (33)] empirically so that the value at the stagnation point on the nose is exact. Lees' result, which is called the "Modified Newtonian Formula," is given by

$$C_p = C_{p_o} \sin^2 \psi \qquad (35)$$

where C_{p_o} is the stagnation point pressure coefficient. The value of C_{p_o} is given by the Rayleigh formula developed from the integral Bernoulli equations and the shock equations and is

$$C_{p_o} = \frac{2}{\gamma M^2} \left[\left(\frac{\gamma + 1}{2\gamma M^2 - \gamma + 1} \right)^{\frac{1}{\gamma - 1}} \left(\frac{\gamma + 1}{2} M^2 \right)^{\frac{\gamma}{\gamma - 1}} - 1 \right] \qquad (36)$$

As in the Newtonian formula, as $M \rightarrow \infty$ and $\gamma \rightarrow 1$, the value of C_{p_o} approaches two.

There are various other modifications to the Newtonian Formula including the Busemann Formula, the Modified Newtonian-Busemann Formula and others but, as is shown in Figures 6 and 7, a comparison of the surface pressure coefficients for the flows over a sphere and a cylinder at $M \rightarrow \infty$ and $\gamma = 1.4$ confirms that the Modified Newtonian
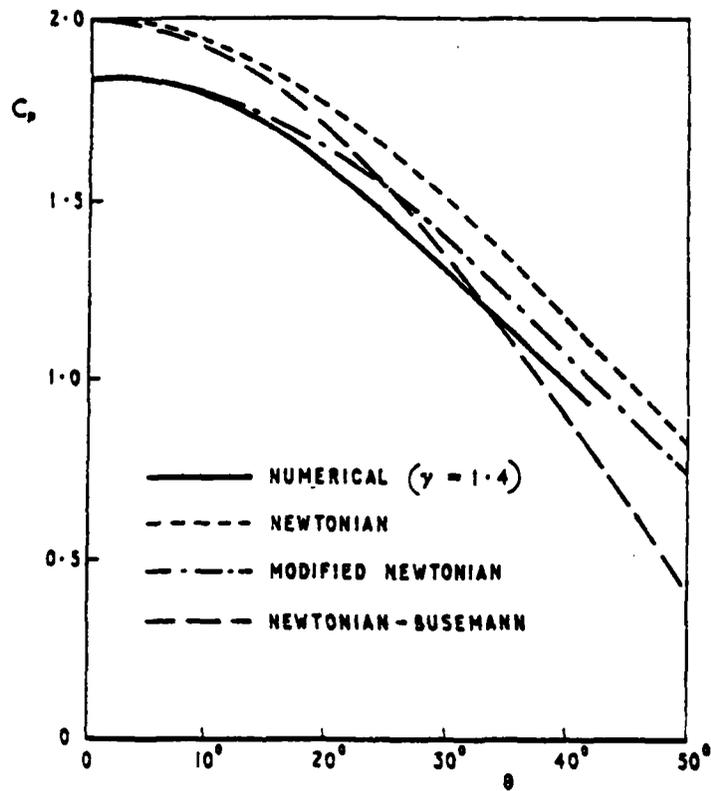
Figure 6. Surface Pressure Distributions for Flow Past a
Sphere (M = ∞, γ = 1.4).
(Reproduced from Cox and Crabtree [Ref. 4],
p. 73).

35
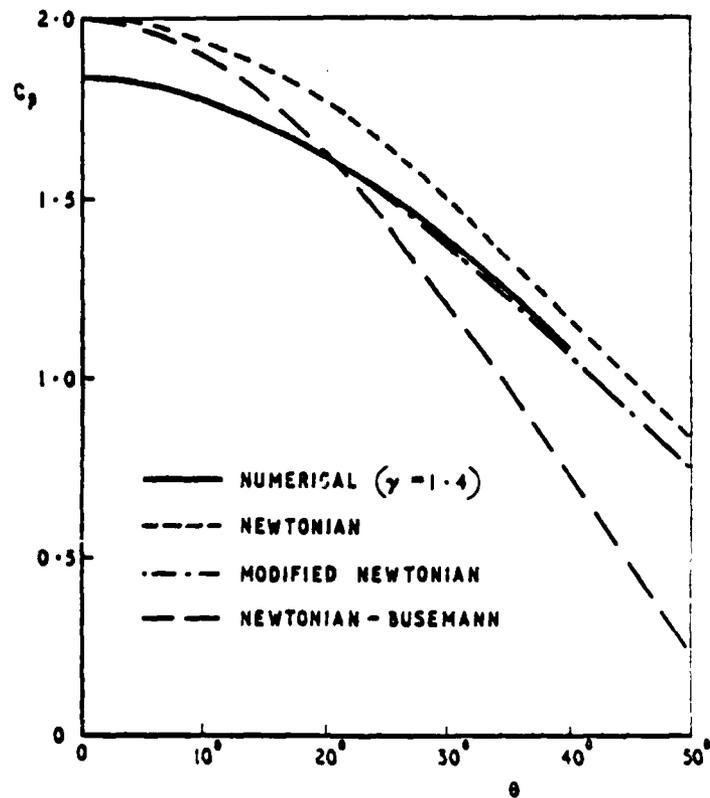
Figure 7. Surface Pressure Distributions for Flow Past a
Circular Cylinder (M = ∞, γ = 1.4).
(Reproduced from Cox and Crabtree [Ref. 4],
p. 72).

Formula is in best agreement with the actual numerical calculations.

1.   Aerodynamic Heating and Ablation

During hypersonic reentry, excessive local heating is a serious problem. For the ballistic vehicle, where the lift-to-drag ratio is zero, very high heat fluxes are encountered but for a relatively short duration, i.e., five to 100 seconds. In practice, the heat and mass transfer phenomena associated with this reentry mode are nonlinear functions of time due to the nonlinear environmental parameters, chemical reactivity, mechanical and acoustical vibration, gas temperature, mode of energy transport, total heat load, peak heating rate, shape of the heat pulse, particle impingement, material properties, etc. Of primary concern is the means of accommodating the energy converted to heat.

The thermal protection of the reentry body can be accomplished in three ways: (a) absorption, (b) radiation, and (c) reduction of aerodynamic heating prior to reaching the vehicle. The added requirement to minimize body weight in order to achieve greater missile range has often led to the choice of materials designed to change phase when heated and to vaporize at the surface exposed to the hypersonic environment. The energy absorption achieved through such processes has proved to be highly effective.

The energy transfer mechanisms between the boundary layer gas and the ablating surface are shown in Figure 8, reprinted from Hurwicz, Kratsch, and Rogan [Ref. 6]. The
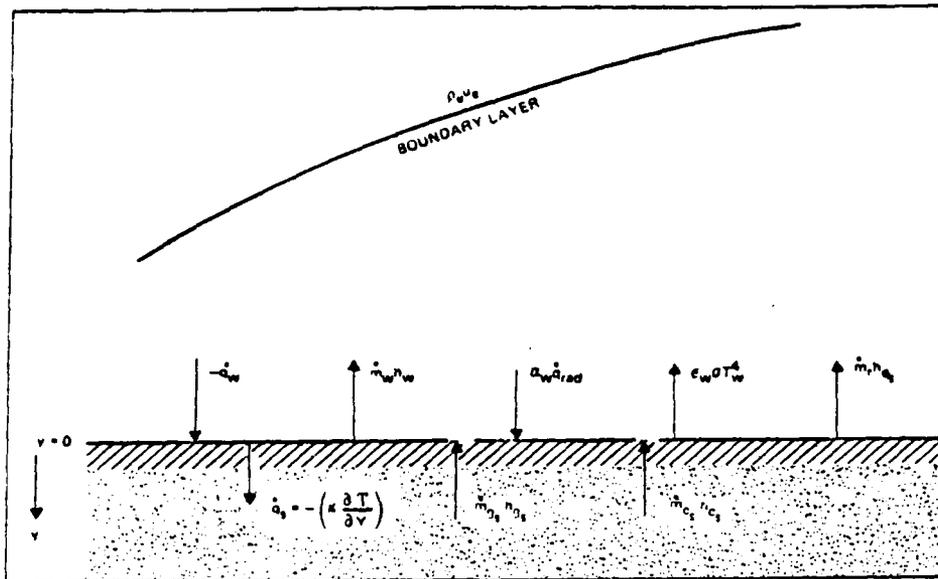
Figure 8.   Heat Flux Balance at the Surface.
(Reproduced from Hurwicz, Kratsch, and Rogan [Ref. 6], p. 9)

energy balance at the surface established the boundary condition for solution of the boundary layer equations. The net heat flux through the surface to the interior of the ablator $(\dot{q}_s)$ equals the summation of the aerodynamic heat flux to the surface from the boundary layer $(-\dot{q}_w)$, the energy transfer away from the surface by normal gas mass flow $(\dot{m}_w h_w)$, the absorption of incident radiation $(\alpha_w \dot{q}_{rad})$, the reradiation of energy from the surface $(+\varepsilon_w \sigma T_w^4)$, the energy transfer by mechanical erosion (ablation) $(\dot{m}_r h_s)$, the energy transfer to the surface by condensed material $(\dot{m}_{c_s} h_{c_s})$, and the energy transfer to the surface by internal gas products $(\dot{m}_{g_s} h_{g_s})$. Note that the aerodynamic heat flux $(\dot{q}_w)$ is the combination

38

of convection to the surface as well as chemical energy
transfer due to surface chemical reactions from mass transfer.
The preceding factors can be expressed as an energy equation

$$\dot{q}_s = -\dot{q}_w - \dot{m}_w h_w + \dot{m}_{c_s} h_{c_s} + \dot{m}_{g_s} h_{g_s} - \varepsilon_w \sigma T_w^4 + \alpha_w \dot{q}_{rad} - \dot{m}_r h_s \quad (37)$$

Equation (37) is applicable for both laminar and
turbulent flow and couples the energy balance to the boundary
layer solution which is required to obtain species concentra-
tions and the heat and mass transfer analysis.

Equation (37), although general, does assume thermo-
chemical equilibrium at the surface and in the boundary
layer. Such equilibrium may not exist in reality since the
mass ablation rate probably is reaction rate controlled by
the ablation material, its char products, and the boundary
layer species. In this case, gaseous ablation products can
be determined in principle through the simultaneous solution
of: (a) all surface thermochemical equilibrium reactions
expressed in partial pressures and equilibrium constants,
(b) equations of conservation of elemental species at the
surface, and (c) Dalton's law of partial pressures.

Even though conceptually the surface thermochemical
equilibrium reactions can be expressed explicitly, the actual
products of the reactions are difficult to determine because
of the elevated temperatures and the number of interacting

39

elements. If, for example, carbon is used as an ablator, the products normally considered are C, C_2, C_3, C_4, C_5, CO, CO_2, CN, O_2, N_2. As can be seen from Figure 9, the concentrations of the gases change as temperature (or velocity) changes. In addition, if water vapor is included, as is of interest in this discussion, another element, hydrogen, must be included as a possible reactant. Thus, entire organic chains of molecules may be formed.
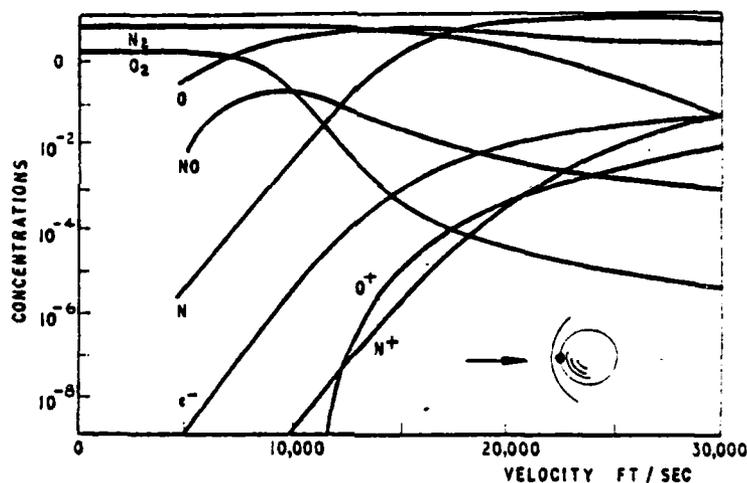
Figure 9. Mole Fraction Concentration behind Normal Shock
(Reproduced from Cox and Crabtree [Ref. 4], p. 10)

In view of the complexity of ablation with non-equilibrium chemical compositions, information concerning nose shape was sought in lieu of direct calculation. Information was found relating nose shape to specific altitudes. The nose tip chosen was composed of a silaceous material.

Ablation occurred during reentry through the atmosphere including mechanical erosion. Further, turbulent flow was assumed to exist from the start of reentry and continue throughout the flight. Figure 10 shows the family of nose shapes selected for this analysis. The material loss due to ablation is excessive compared to modern carbon nose tips; however, the effects of nose shape change on the trajectory were to be examined. Therefore, the larger the ablation rate, the more the trajectory could be expected to change from the non-ablating entry.
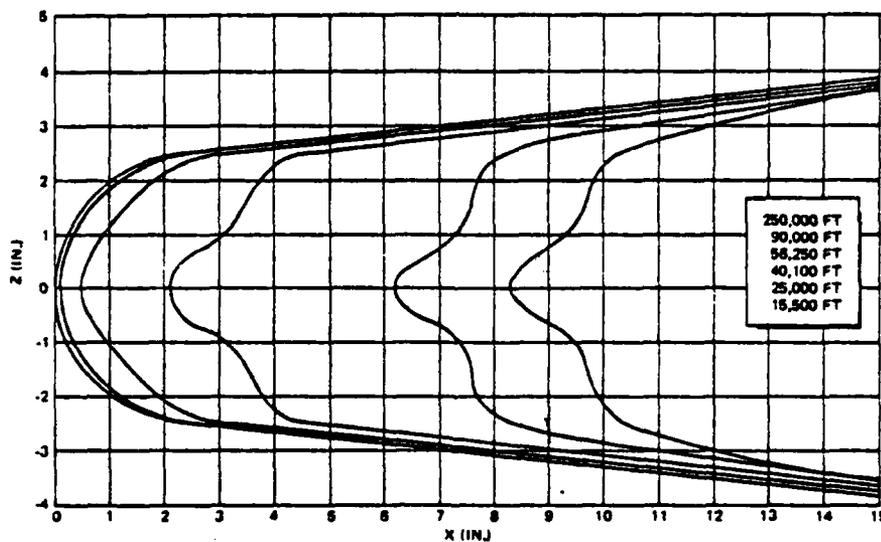
Figure 10.   Nose Shape of Reentry Body at Various Altitudes. (Reproduced from Hurwitz, Kratsch, and Rogan [Ref. 6], p. 16).

Recent experiments have shown that interesting after-body ablation patterns are formed during reentry.

41

Cross-hatching or other similar spiral ablation patterns
occur, and related roll torques are induced producing erratic
perturbations in roll behavior. Such phenomena were not
considered in this analysis.

   2. Drag

      The drag of a reentry body experiencing Newtonian
flow can be expressed as:

$$\text{Drag} = q \int_A C_p \sin\psi \ dA \qquad (38)$$

where q represents dynamic pressure, C_p represents pressure
coefficient, ψ is the local slope of the body, and A is an
element of area. Given the nose shapes in Figure 10 and
assuming that the shape of the nose can be determined for
every altitude, the drag at any altitude can be computed
using equations (35) and (36). For an axisymmetric body
where $r = f(x)$, the body can be divided into infinitesimal
segments of X; and the drag can be found on each elemental
circular element. Figure 11 shows a typical element in the
x-r plane. Figure 12 shows the same element as seen along
the longitudinal axis and where R is the base radius of the
reentry body. Therefore, the incremental area is

$$dA = 2\pi r ds = \frac{2\pi r \ dr}{\sin\psi} \qquad (39)$$
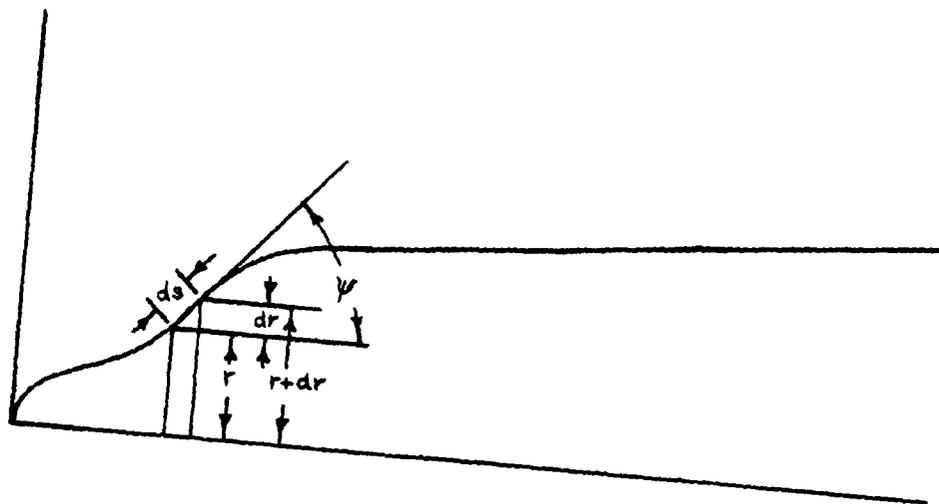
Figure 11.   Cross-Section of Elemental Area along the Nose.
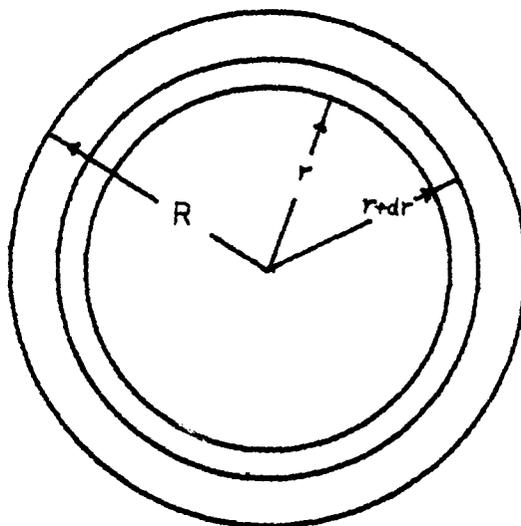
Figure 12.   Front View of Elemental Area along the Nose.

43

Hence, equation (38) can be written for the elemental drag
and becomes

$$d(\text{Drag}) = q \int_{r}^{r+dr} C_p \; 2\pi r \, dr \qquad (40)$$

The total drag on the body is then the sum of the
elemental drags over the length.

$$\text{Drag} = \sum_{x=0}^{x=L} q C_p \pi (r_2^2 - r_1^2) \qquad (41)$$

Since the Newtonian flow model applies over the
length of the nose, the "afterbody" can be included in the
nose shape equations if properly written; hence equations (38)
to (40) will define the drag in all regions along the body.

For projectiles which fly at low supersonic velocities,
the base drag is very important when considering the total
drag on the body. However, at hypersonic velocities, the
pressure increase across the shock at the nose is so large,
of the order of one hundred atmospheres, that the low pressure
at the base of the reentry body is comparatively insignificant.
In this analysis, the base pressure drag was neglected.

C. HUMIDITY EFFECTS

As noted previously, the effects of water vapor, water droplets and ice crystals in the atmosphere lead to extremely complex modifications to all the equations previously cited. Considering water vapor only, density of the air is changed. As a result, the modified density influences reentry body velocity, ablation rate, etc. Also, as mentioned before, more complex chemical equations are required to determine ablation products and, hence, heat loss and absorption. The total effect on drag, for instance, would be the sum of the effects on each parameter affecting drag; for example:

$$\frac{\Delta \text{ Drag}}{\text{Drag}} = \frac{\Delta \text{ density}}{\text{density}} + \frac{\Delta C_p}{C_p} + \frac{\Delta q}{q} + \frac{\Delta \text{ area}}{\text{area}} \qquad (42)$$

If rain, i.e., suspended water droplets, also is included in the analysis, mechanical erosion must be considered. Additionally, when the droplets cross the shock wave in front of the vehicle, scattering and annihilation will occur; and only some fraction of the droplet mass actually will contact the surface of the body. The interaction of water vapor and rain with the reentry body is not considered in this thesis.

The interaction of ice in high altitude clouds would seem to be a worse case of humidity effect interaction with a reentry vehicle since the assumption can be made that most of the typical ice particles will survive after passing through the

45

shock front. Hence, mechanical erosion should be increased greatly. Experiments have shown that the mass ablated can be many times the impact mass of the typical ice particle.

Equations also are simplified since the time in the boundary layer is so short, of the order of microseconds, that the ice will not undergo a change in phase before colliding with the body. Therefore, changes in ice crystal properties and chemical interactions were neglected.

Since information was not available concerning the actual change in nose shape due to collisions with ice particles, the assumption was made that ablation shape was not changed but merely was increased in rate of mass loss. That is, the identical equations describing the nose shape were used in both the baseline trajectory model and the ice cloud trajectory model. However, as mass loss increased due to impact, the nose shape was changed according to those equations until the proper mass loss was achieved. This assumption is no doubt incorrect in that it would be expected that the mass loss would be much greater near the stagnation point and much less along the perimeter of the body.

III. SIMULATION

A. BASELINE TRAJECTORY

In order to evaluate the consequences of reentry through
ice clouds, a reference trajectory was needed to compare such
parameters as range, impact velocity, changes in drag coeffi-
cient, etc. The equations of motion were presented previously,
but initial conditions and boundary conditions are required
to solve for a specific trajectory.

1. Selection of a Typical Reentry Vehicle

The model selected as the reentry vehicle conforms
to the nose shapes shown in Figure 10. In addition, realistic
values of ballistic coefficient and drag coefficient were
required. Modern ballistic reentry vehicles have ballistic
coefficients (weight divided by the quantity drag coefficient
times base area) in the range of 1500-2000 pounds per square
foot and drag coefficients slightly greater than 0.1.

The weight of the reentry vehicle was not known,
but a specific gravity of 1.4 was selected as typical.
During the course of the initial iterations of the computer
model, the body length was changed to add enough mass so that
the ballistic coefficient was near the desired value of 2000.
The body shape was achieved by extending the after-section of
the initial nose shape shown in Figure 10. Figure 13 shows
the final model shape prior to reentry.
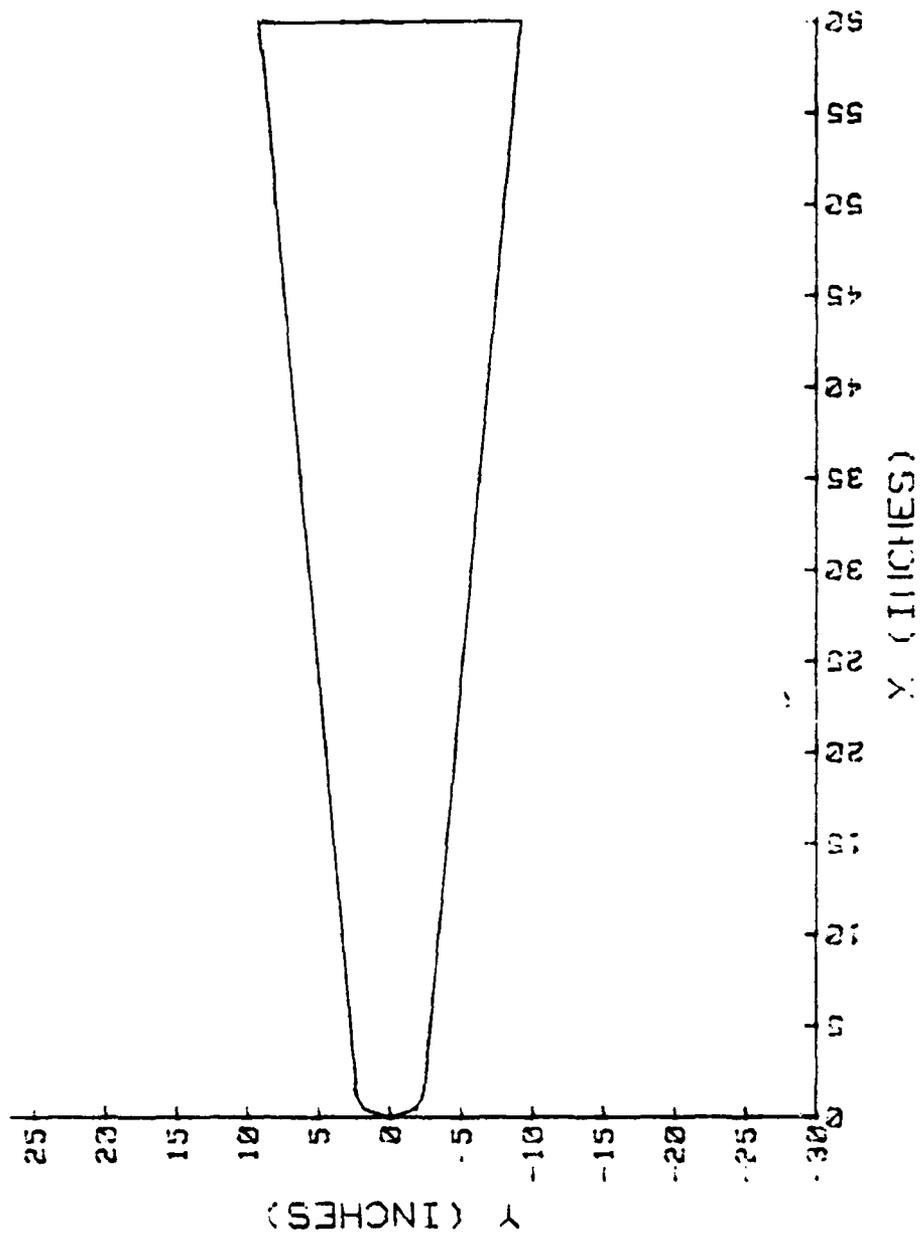
Figure 13. Model Reentry Vehicle Shape

48

2. Initial Conditions

Referring to Figure 4, the center trajectory was chosen as a representative trajectory of a typical Navy reentry vehicle which might be launched by Polaris or Trident. This curve corresponds to a maximum range of about 4100 nautical miles if launched at an angle of 27° with an initial velocity of 22006 feet per second. Substituting the values for launch angle and initial velocity, equation (20) yields $K = 9.15 \times 10^8$ ft^2/sec^2 as shown previously.

Since deceleration and ablation have not yet begun at 250,000 feet, this altitude was chosen as the initial altitude to begin reentry. For an altitude of 250,000 feet, the value of r, the distance to the center of the earth, is 2.115×10^7 feet; the value for r was substituted into equation (21) to yield

$$V_\phi = [2(K + gr)]^{1/2} = 2[\ 9.15 \times 10^8 - 32.2(2.115 \times 10^7)]^{1/2}$$

$$= 21,632 \text{ ft/sec} \tag{43}$$

At an altitude of 250,000 feet atmospheric density is too low to cause drag. Also, at that altitude r is not much different from R, the radius of the earth. Therefore, the coordinate system can be shifted from r,θ to x,y. Since x forces are zero, the x component of velocity will remain constant and

will be equal to the launch velocity times the cosine of the launch angle

$$V_x = V_\phi \cos A = 22006 \cos 27° = 19,607 \text{ ft/sec} \qquad (44)$$

At 250,000 feet, the x-component of velocity must be the same value; and since the value of V is known, the reentry angle A can be determined from

$$A = \cos^{-1} \frac{V_x}{V_\phi} = \cos^{-1} \frac{19607}{21632} = 25.04° \qquad (45)$$

Checking these values with the curve selected in Figure 10 and using equation (18),

$$\cos \theta_0 = \frac{1 - 2(.6)^2 \cos^2(27°)/1}{[1 + 4(.06)^2 \cos^2(27°)(.6^2 - 1)]^{1/2}} = 0.827$$

Therefore, the initial angular distance from apogee is $\theta_0 = 34.21°$. Thus total range using equation (19) is

$$\text{Range} = 2R\theta_0 = \frac{2(2.09 \times 10^7)}{6000} \frac{(34.21)\pi}{180} = 4160 \text{ nm}$$

which corresponds very well to the expected value of 4100 nm.

50

The range the reentry vehicle is expected to fly can be found from the reentry location to impact. To find the range for a no-drag trajectory recall that the arc length traveled is

$$\theta' = \theta_0 - \theta \tag{46}$$

Again, using equation (18) and substituting values for V, A, and r' at the entry point

$$\cos\theta = \frac{1 - 2(.6)^2\cos^2(25.04°)/(1.01)}{[1 + 4(.6)^2\cos^2(25.04°)(.6^2 - 1)]^{1/2}} = 0.843$$

$$\text{and } \theta = \cos^{-1}(.843) = 32.54°.$$

The angular arc of flight using equation (46) is

$$\theta' = \theta_0 - \theta = 34.21° - 32.54° = 1.67°$$

and using equation (19)

$$\text{Range} = R\theta' = \frac{(2.09 \times 10^7)}{6000}\frac{(1.67)\pi}{180} = 101.5 \text{ nm}$$

Since the sequence of equations above assumed no drag, the
range should be the maximum expected range of the model
reentry vehicle.

Table 3

Summary of Initial Conditions at
an Altitude of 250,000 Feet

Initial Velocity	21,632 ft/sec
Initial Entry Angle	25°
Initial x velocity	19,607 ft/sec
Initial y velocity	9,138 ft/sec
Maximum range	101.5 nm

3. Nose Shape

The nose shape is the primary factor in determining
total vehicle drag. Since the nose shape was given only for
discrete values of altitude as in Figure 10, the nose shape
was constructed artificially as a continuous function of
altitude. This was done by using the HP-9845A computer along
with the HP-9874A Digitizer. Each of the six nose shapes was
divided into two segments; one segment was from the nose tip
to 2.4 inches aft of the nose tip, and one segment was from
2.4 inches aft of the nose tip to about 20 inches aft of the

nose tip. Another function was required to describe the recession of the nose tip.

Each nose shape was traced with the digitizer inputting data points into the computer. A curve fitting routine was used to construct curves of nose radius as a function of length along the centerline of the reentry body using the data from the digitizer. The best fit curve for the segments from the nose tip to 2.4 inches aft of the nose tip was a fifth-order polynomial with constant coefficients. The segment from 2.4 inches aft of the nose tip was described by a straight line. Appendix A contains graphs of each of the six nose shapes (two segments each) comparing the data input with the plot of the equations which describe the data. As can be seen, the graphs very closely approximate the actual nose shapes.

The nose shapes thus were defined mathematically as

$$r = \sum_{i=0}^{5} A_i x^i \tag{47}$$

for $0 \leq x \leq 2.4$ inches and as

$$r = \sum_{i=0}^{1} B_i x^i \tag{48}$$

53

for x > 2.4 inches where r is the local radius of the

reentry body and x is the distance along the centerline.

Using the coefficients calculated in equations (47)

and (48), plots of each coefficient versus altitude were

constructed. For example, all the fifth-order coefficients

of equation (47) were plotted at the altitudes applicable

to the particular nose shapes. The coefficients in equation

(47) thus were defined by

$$A_i = \sum_{j=o}^{6} C_{ij} h^j \tag{49}$$

where h is altitude in feet. The coefficients in equation

(48) were defined by

$$B_i = \sum_{j=o}^{6} D_{ij} h^j \tag{50}$$

Division of the coefficient curves into two portions was

necessary; equations (49) and (50), sixth-order polynomials,

applied below 90,000 feet. Equations (51) and (52)

$$A_i = \sum_{j=o}^{1} E_{ij} h^j \tag{51}$$

$$B_i = \sum_{j=0}^{1} F_{ij}h^j \tag{52}$$

were used above 90,000 feet.

Equations (47) through (52) can be combined to yield the nose shape, the radius, as a function of altitude in the various regions of applicability. Table 4 shows the combined equations (53) through (56) and the regions of applicability.

Table 4

Summary of Nose Shape Equations

Altitude	$0 \leq x \leq 2.4$ (inches)	$x > 2.4$ (inches)
Equal to or Below 90,000 feet	$r = \sum_{i=0}^{5} \sum_{j=0}^{6} C_{ij}h^j x^i$ (53)	$r = \sum_{i=0}^{1} \sum_{j=0}^{6} D_{ij}h^j x^i$ (54)
Above 90,000 feet	$r = \sum_{i=0}^{5} \sum_{j=0}^{1} E_{ij}h^j x^i$ (55)	$r = \sum_{i=0}^{1} \sum_{j=0}^{1} F_{ij}h^j x^i$ (56)

Appendix B compares graphs of the polynomials describing the A_i coefficients versus altitude with corresponding graphs of the digitizer data input used. Appendix C contains similar graphs of the nose tip recession versus altitude. All graphs show that the equations adequately represent the described data.

55

The result of the above analysis was to allow the insertion of any altitude into equations (53) through (56), yielding the corresponding nose radius as a function of the centerline distance from the nose tip.

4. Flow Chart

Using the initial entry conditions and nose shape versus altitude information previously described along with the equations of motion, a program to calculate trajectory was possible. Figure 14 describes the process.

5. Validity

The program initially was modified to print the nose shapes every second along the trajectory so that a comparison between the desired nose shapes described in Figure 10 and the nose shapes described by the equations derived in Section IIIA3 could be made. Figure 15 shows a family of curves plotted from the program output for nose shape at altitudes closely corresponding to the altitudes for the family of curves in Figure 10. Although the nose shapes in Figure 15 are somewhat more square in appearance than those in Figure 10, the proper general shapes were clearly achieved with the nose shape as a function of altitude equations.

A goal of the model was to achieve a drag coefficient of about 0.1 and a ballistic coefficit of about 2000. In the simulation, the drag coefficient ranged from 0.100 to 0.127 during the flight with the initial value of 0.105. The ballistic coefficient ranged from 1392 to 1878 during the flight with the initial value of 1798. The range should be

56

```
  ( Start )  ───────►  ┌─────────────────────────────────────┐
                       │ Initial Inputs; Altitude, Velocity,  │
                       │ Reentry Angle,                       │
                       │ Nose Shape Coefficients              │
                       │                                      │
                       │ k=0 (Program Counter)                │
                       └─────────────────────────────────────┘
```

┌───────────────────┐   ┌────────────────────┐ Eqn(1),(26)to(30)   ┌──────────┐
│ Change variables │   │ Calculate new vel- │   │ Print   │
│ x1=x2   │   │ ocity, density,   │◄────────────────────────────┤   │
│ y1=y2   │   │ dynamic pressure, │   └──────────┘
│ x2=x3   │   │ Mach number   │
│ y2=y3   │   └────────────────────┘
└───────────────────┘

┌───────────┐   ┌────────────────────┐ Con. (36),
│   k=1   │   │ Calculate C_{p_0} │ (53)to(56)
└───────────┘   │ Calculate nose   │
                │ shapes   │
┌────────────────┐   └────────────────────┘
│ Altitude=0   │
│ Calculate range│   ┌────────────────────┐
└────────────────┘   │ Calculate C_p, drag,│
                     │ volume, mass,   │
         No   │ C_D, β │
      ◇ Altitude<0 ◇ └────────────────────┘
  Yes

                     ┌────────────────────┐ Eqn(44),
                     │ Calculate current │ (45)
                     │ entry angle,   │
                     │ velocity   │
                     └────────────────────┘

                     ┌────────────────────┐
                     │ Increment time   │
                     └────────────────────┘

┌────────────────┐   ┌──────────┐
│ Calculate new │   No   │ Print   │
│ altitude   │◄── ◇ k=1 ◇ ──► Yes ┌────────┐   (Stop)
└────────────────┘   │ Print │──────►
                                       └────────┘

Figure 14.   Flow Chart of Baseline Trajectory Program

(Note: Nose shapes progressing from left to right correspond to altitudes progressing from top to bottom.)

250,000 ft.
89,658 ft.
53,230 ft.
37,003 ft.
25,563 ft.
13,396 ft.

X (INCHES)

Y (INCHES)
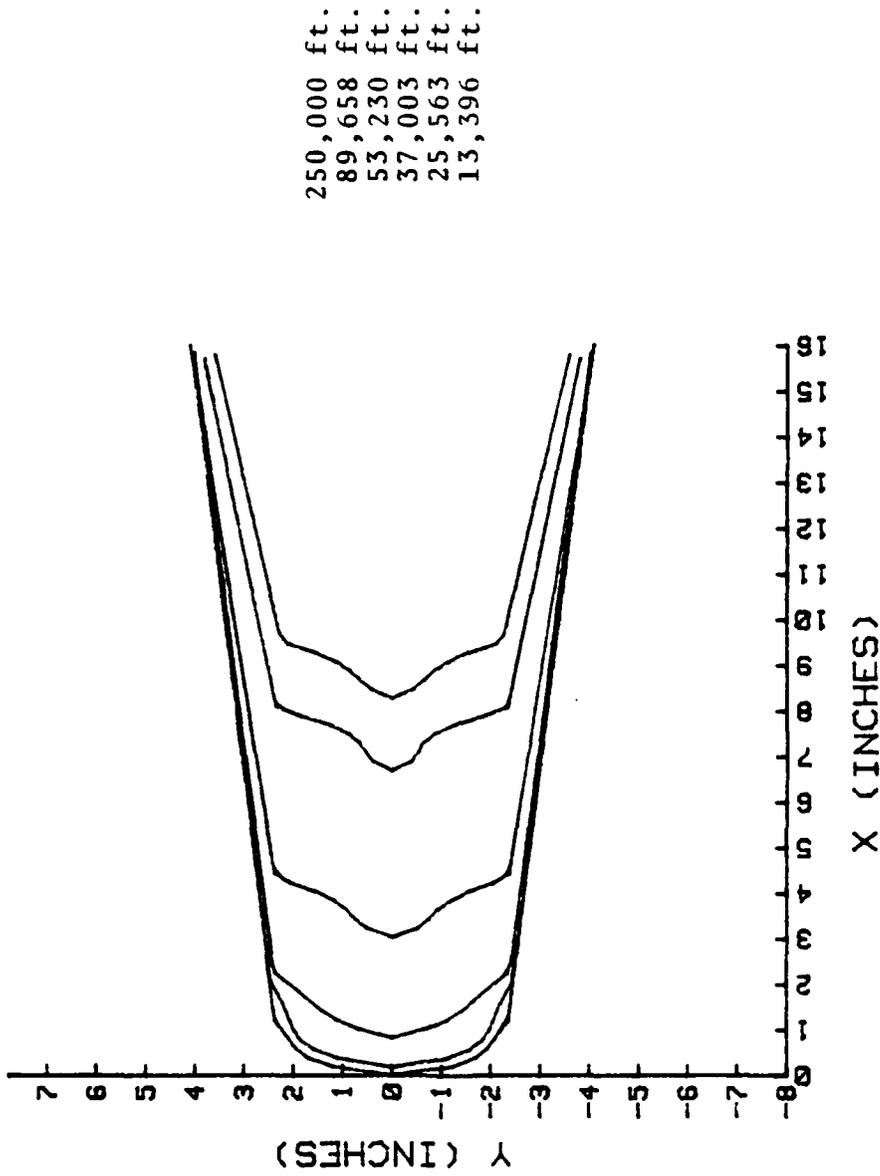
Figure 15. Nose Shapes at Various Altitudes

less than the vacuum trajectory range of 101.5 nm; the range with drag was 84.103 nm.

For ballistic entries at escape velocity and initial angles of inclination greater than about 5°, the variation of velocity with altitude has been computed by Loh [Ref. 7] for various values of ballistic coefficients. Figure 16 shows a plot of the various deceleration curves. A similar curve can be generated from the simulated reentry. The generated curve should be the same shape as Figure 16 but since the reentry velocity is only about 80 percent of escape velocity, all values of dimensionless velocity will be lower.

In addition, the simulated reentry body undergoes ablation and hence changes the value of the ballistic coefficient. However, if a nominal ballistic coefficient of 1500 is chosen, the value of

$$\frac{C_D A}{W \sin\theta} = \frac{1}{\beta \sin\theta} \cong \frac{1}{1500 \sin 25°} = 0.0016 \qquad (57)$$

can be used, where θ corresponds to reentry angle. Qualititatively, the simulated reentry curve should lie between the 0.001 and 0.01 curves and to the left of the curves in Figure 16.

Figure 17 is a graph of the Mach number versus altitude for the model. Maximum deceleration occurs at

59
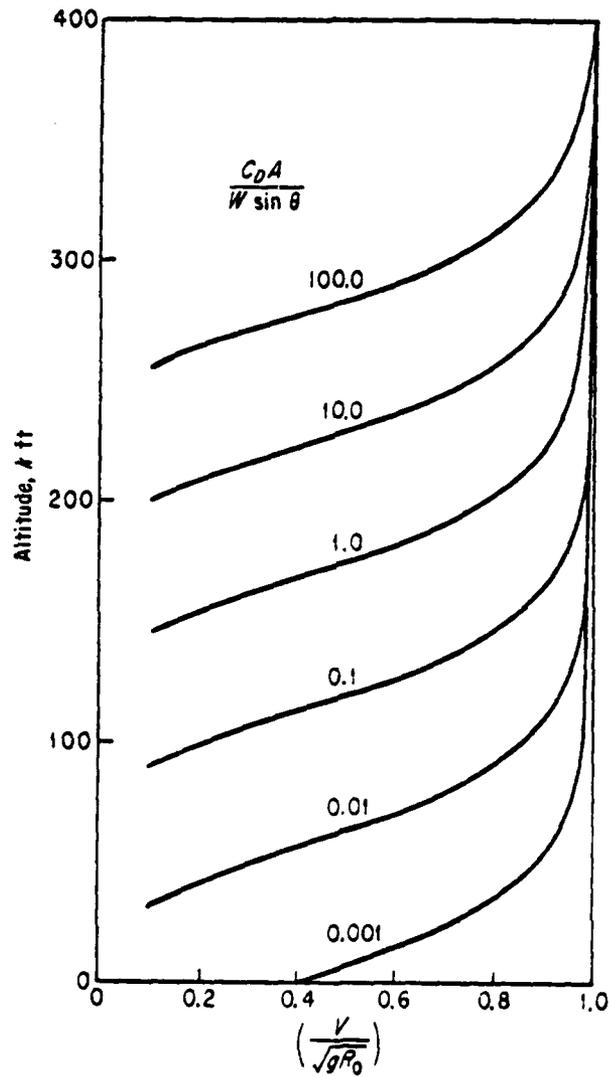
Figure 16.   Velocity Variation during Direct Penetration of
the Earth's Atmosphere.

(Reproduced from Loh [Ref. 7], p. 110)
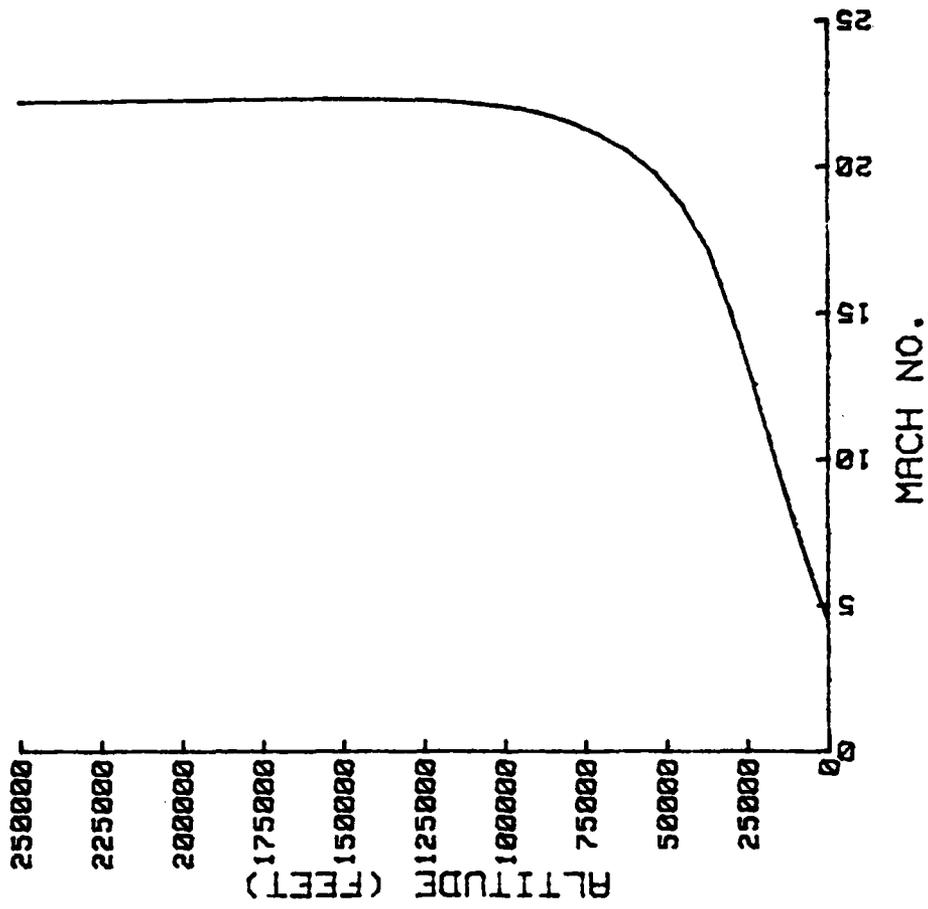
Figure 17. Altitude versus Mach Number

61

about 75,000 feet, and the actual impact Mach number is 4.42. Based on the above parameters and the similarity in shape between curves in Figures 16 and 17, the computer model was accepted as a valid representation of the actual reentry trajectory.

B. TRAJECTORY THROUGH AN ICE CLOUD

1. Model Cloud

In order to evaluate realistically the effects of ice clouds on the trajectory of a reentry body, a representative ice cloud was needed. Such information as altitude, thickness, particle size and concentration was needed. Although information such as this is readily available for relatively low altitude rain clouds, useful information regarding high altitude ice clouds is very rare. The only information found is contained in Table 5, reproduced from Heymsfield [Ref. 8], in which aircraft measurements of five different cirrus uncinus clouds were made.

Table 5

Summary of Cloud Measurements
(Reproduced from Heymsfield [Ref. 8], p. 800)

Flight no.	Date	Cloud type	Cirrus altitude (km)	Sampling altitude (km)	Sampling temperature range (°C)	Ice water content* (gm m⁻³)	Concentration Total (cm⁻³)	Concentration Average larger than 0.15 mm (cm⁻³)	Calculated reflectivity factor* (mm⁶ m⁻³)	Calculated precipitation rate* (mm hr⁻¹)	Mean crystal (mm) length
14	9 July 1970	Ci unc	6.5-8.8	6.5-8.0	-15 to -30	0.19 0.24	—	0.019	17 9	1.0 0.6	0.9
C-1	19 Sept 1971	Ci unc	8.5-9.1	8.5-9.1	-36 to -43	0.39 0.24	—	0.025	36 14	1.6 0.7	0.75
C-21	19 Sept 1971	Ci unc	8.9-9.35	8.9-9.35	40 to -44.5	0.25 0.15	—	0.03	14 7	0.97 0.5	0.75
G-11	6 Apr 1972	Ci unc	9.6-11.0	9.6-11.0	-41.7 to -57.6	0.44 0.30	0.40	0.03	20 10	1.0 0.6	0.6
G-21	6 Apr 1972	Ci unc	9.8-10.1	9.8-10.1	-43 to -46	0.30 0.20	0.20	0.04	12 9	0.9 0.6	0.5
G-31	6 Apr 1972	Ci unc—Cs	9.35-9.8	9.35-9.8	-14 to -45	0.16 0.075	0.30	0.015	14 4	0.7 0.2	0.5
117	4 Mar 1972	Cs	4.45-8.5	4.45-7.9	-20 to -46	0.007 0.026	—	0.008	4.3 0.5	0.3 0.1	0.35
E	4 Apr 1972	Cs	7.9-8.9	7.9-8.4	-35 to -44.5	0.04 0.025	0.20	0.004	0.6 0.4	0.1 0.025	0.35

The table shows that the clouds ranged in altitude from 4.45 to 11 kilometers (14,600 to 36,100 feet) and varied in thickness from 0.3 to 3.45 kilometers (980 to 11,300 feet). Based upon the above figures and the advice of Dr. K. L. Davidson, Meteorology Department, Naval Postgraduate School, the representative ice cloud was selected to be at an altitude of 30,000 feet with a thickness of 5,000 feet. Ice particle concentration at that altitude nominally was chosen as 0.24 gram per cubic meter which corresponds to 4.65×10^{-7} slug per cubic foot.

2. Mass Defect

The mass of the reentry body ablated by collision with the ice particles can be expressed by

$$\text{Mass Defect} = \frac{\text{Base area x Cloud thickness x Mass Loss Factor}}{\cos A} \quad (58)$$

where the base area of the reentry body and the angle of the trajectory with respect to the horizontal, A, are computed at the proper altitude by the computer program. The Mass Loss Factor represents the ratio of the mass ablated to the mass of the ice particles which collide with the body. Some information for Mass Loss Factor exists for multiple impacts without a shock wave ahead of the reentry body, but none could be found which included the shock wave. Therefore, several nominal values of Mass Loss Factor were selected, and the

63

matrix of 10, 20, 30, and 40 was computed. A trajectory
was calculated for each.

One assumption inherent in equation (58) is that all
of the ice particles contained in a tube representing the
ba_. area of the reentry body passed at the proper angle
through the cloud thickness do impact on the body. Such an
assumption was made since this analysis was based on a worst
case scenario. If only a portion of the ice impacts on the
body, which is the more likely case, less ablation will occur
and, therefore, less of an effect will result.

3. Flow Chart

Using the cloud information contained in Table 5
and equaticn (58), the flow chart in Figure 14 was modified
to include ablation due to ice erosion. Figure 18 describes
the process.
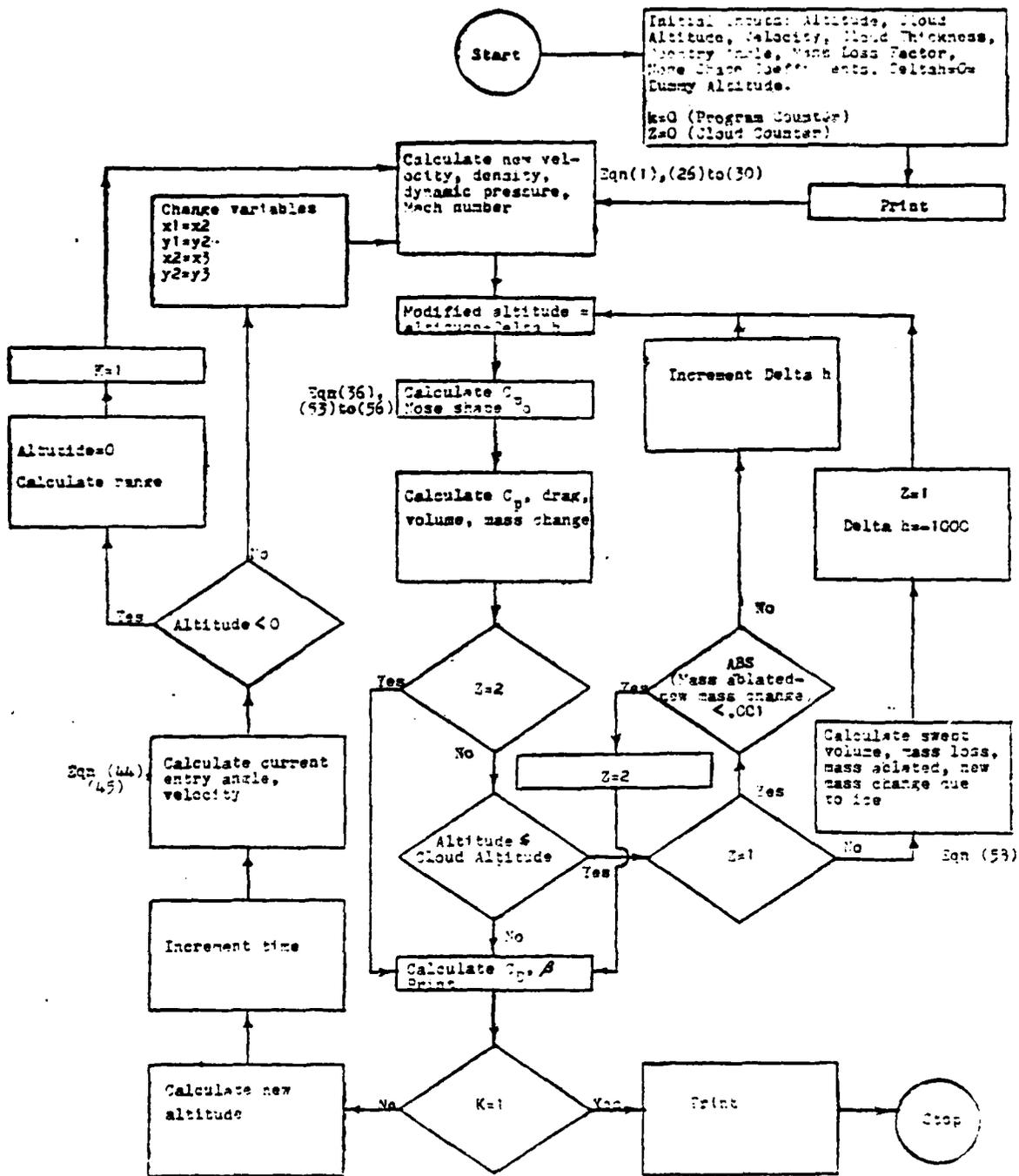
Figure 18. Flow Chart of Trajectory Program with Ice Cloud Ablation

IV. RESULTS, CONCLUSIONS AND RECOMMENDATIONS

A. RESULTS

Table 6 compares the difference in range of the various trajectories modeled as functions of Mass Loss Factor, which is the ratio of mass loss of ablation material due to erosion to the mass of ice particles impacting. Also shown are the values of mass loss due to ice erosion and final Mach number. Figure 19 shows the same results graphically.

Table 6

Comparison of Trajectories with Ice Erosion
to Baseline Trajectory

Mass Loss Factor	Final Mach Number	Mass Loss Due to Ice (slugs)	Difference in Range (feet)
0	4.417	0	0
10	4.418	0.0947	1.54
20	4.420	0.1895	2.85
30	4.425	0.2842	7.99
40	4.429	0.3789	15.03

B. CONCLUSIONS

The most interesting result of the analysis is that the reentry vehicle with ice erosion traveled farther in all cases than did the vehicle without ice erosion. The reason is that, despite the significant mass loss due to erosion which tends to decrease the ballistic coefficient, the final

66
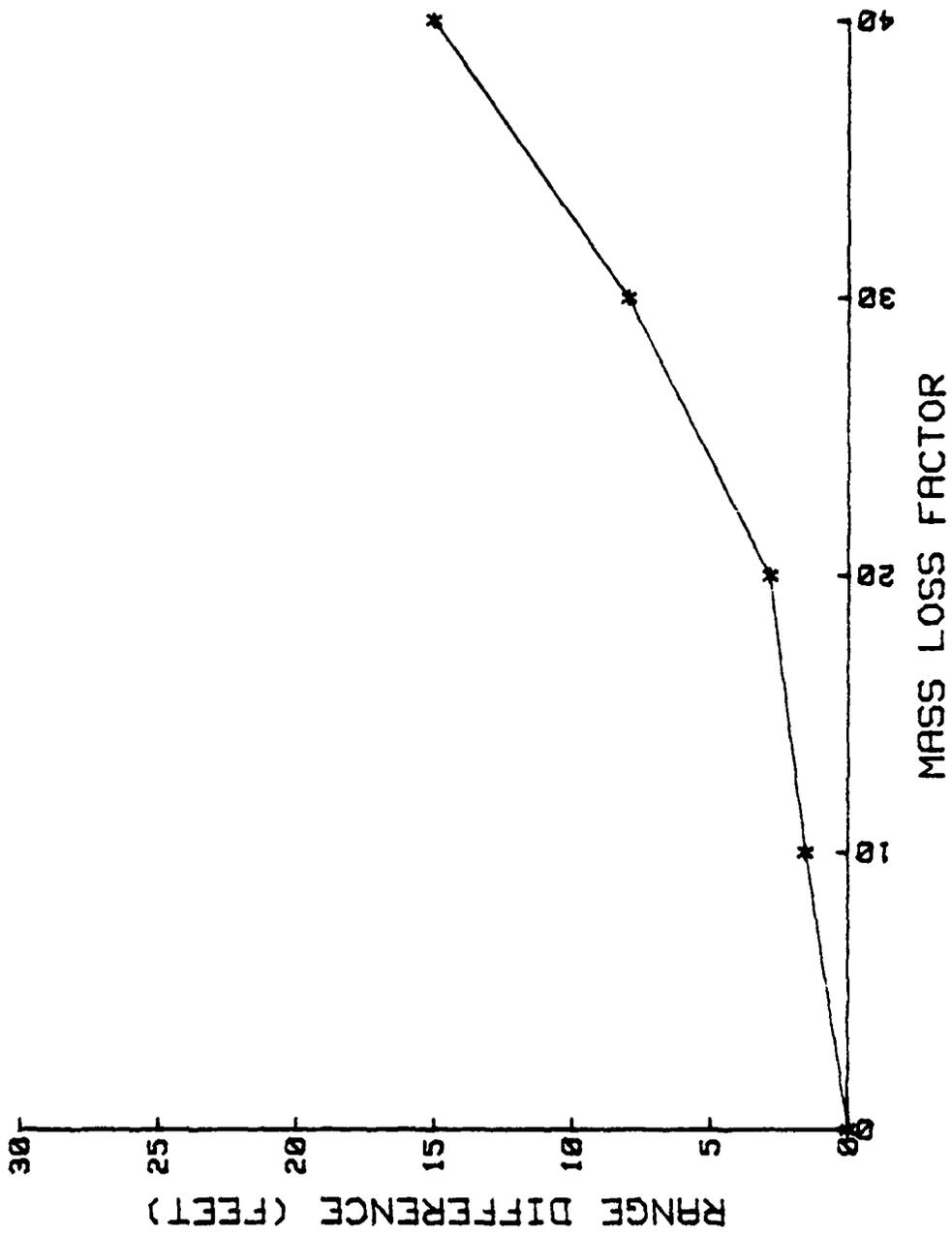
Figure 19. Range Difference versus Mass Loss Factor

67

nose shape, as seen in Figures 10 and 15, reduces the drag coefficient and tends to increase the ballistic coefficient. The result is that the two parameters, mass loss and drag coefficient, are of opposite sign and tend to cancel.

Circular Error Probability, CEP, is a constant multiplied by the variance in range, and for a Gaussian distribution

$$\sigma^2 = \sum_i \sigma_i^2 \tag{59}$$

where σ_i denotes the variance in range caused by the various factors that influence changes in range. The assumption can be made that another σ_i, that is, the variance due to ice erosion, can be added to equation (59) and further that the variance due to ice erosion is of the order of the change in range due to ice erosion. If it also is assumed that the CEP is of the order of the variance, then equation (59) can be written

$$CEP^2 = \sum_i CEP_i^2 = CEP_1^2 + \Delta\ Range^2 \tag{60}$$

where CEP_1 is the original CEP of the body due to all factors excluding ice erosion and Δ Range is the difference in range due to ice erosion. For a C-4 Trident with an initial CEP of 1500 feet (from Table 2) and a Mass Loss Factor of 40 for a Δ Range of 15.03 feet, equation (60) yields a new CEP of 1500.08 feet.

68

The assumptions in this thesis were made on the basis of the best information available in the literature. The analysis of the problem based on the assumptions indicates that the difference in CEP due to ice erosion is very small indeed. Considering ice erosion as the worst case for atmospheric water phenomena, the CEP change due to water droplet erosion or due to differences in humidity also can be considered to be very small.

C. RECOMMENDATIONS FOR FUTURE WORK

1. The nose shape after impact with ice particles is obviously very important. Experiments which measure the effects of multiple collisions of ice on nose shape are required. Such experiments must include the effects of a bow shock around the nose equivalent to a Mach number of about 10. Conceptually, more ice should impact near the centerline of the vehicle and less toward the edges, tending to make the body more blunt and therefore tending to increase the drag coefficient.

2. This analysis should be redone using data for a carbon-carbon nose and new data for ice erosion found in part 1 above. The mass loss for a carbon-carbon nose tip would tend to be far less than for the silaceous nose tip which is modeled in this thesis. Hence, mass loss due to general erosion would tend to have less effect than in this analysis.

It may be, however, that the mass loss due to ice erosion for the carbon-carbon nose is of the same order of magnitude as the mass loss due to ice erosion for the silaceous nose. If so, the effects of ice erosion may be more important in the carbon-carbon nose than in the silaceous nose because the effects of mass loss due to ice erosion were masked in the silaceous nose by the substantial mass loss occurring throughout the reentry.

APPENDIX A

POLYNOMIAL REPRESENTATION OF NOSE SHAPES

The following pages contain graphs of the various nose shapes. Each graph contains a plot of the data points taken from the respective nose shape curves in Figure 10 with the aid of the HP-9874A digitizer and a plot of the polynomials which describe the data points. The polynomials also are displayed on the graph; the fifth-order polynomial applies for $0 \leq x \leq 2.4$ and the first-order polynomial applies for $x > 2.4$.

In the analysis, the polynomial was used to describe the first 2.4 inches of the nose shape. The linear approximation was used to describe the nose shape from 2.4 inches aft of the nose tip to about 20 inches aft of the nose tip. The linear approximation to Figure A-1 was used to describe the nose shape from about 20 inches aft of the nose tip (where the two linear portions intersect) to the end of the reentry body for all nose shapes.

The profiles for nose shapes with ice erosion use the same equations to describe the shape. The coefficients are modified by substitution of a modified altitude into the equations for the coefficients displayed in Appendix B.

$$0 \leq X \leq 2.4$$

POLYNOMIAL MODEL: $Y = A(M) * X^{(M-1)} + \ldots + A(1) * X + A(0)$

Coefficients:
A(0)=0.1615513?
A(1)=7.12021/03
A(2)=-11.0821419
A(3)=8.5315763
A(4)=-3.0413/139
A(5)=0.4022848/

$$X > 2.4$$

LINEAR MODEL: $Y = A + B * X$

A=2.22/1434/368
B=0.116104982804

X (INCHES)

Y (INCHES)
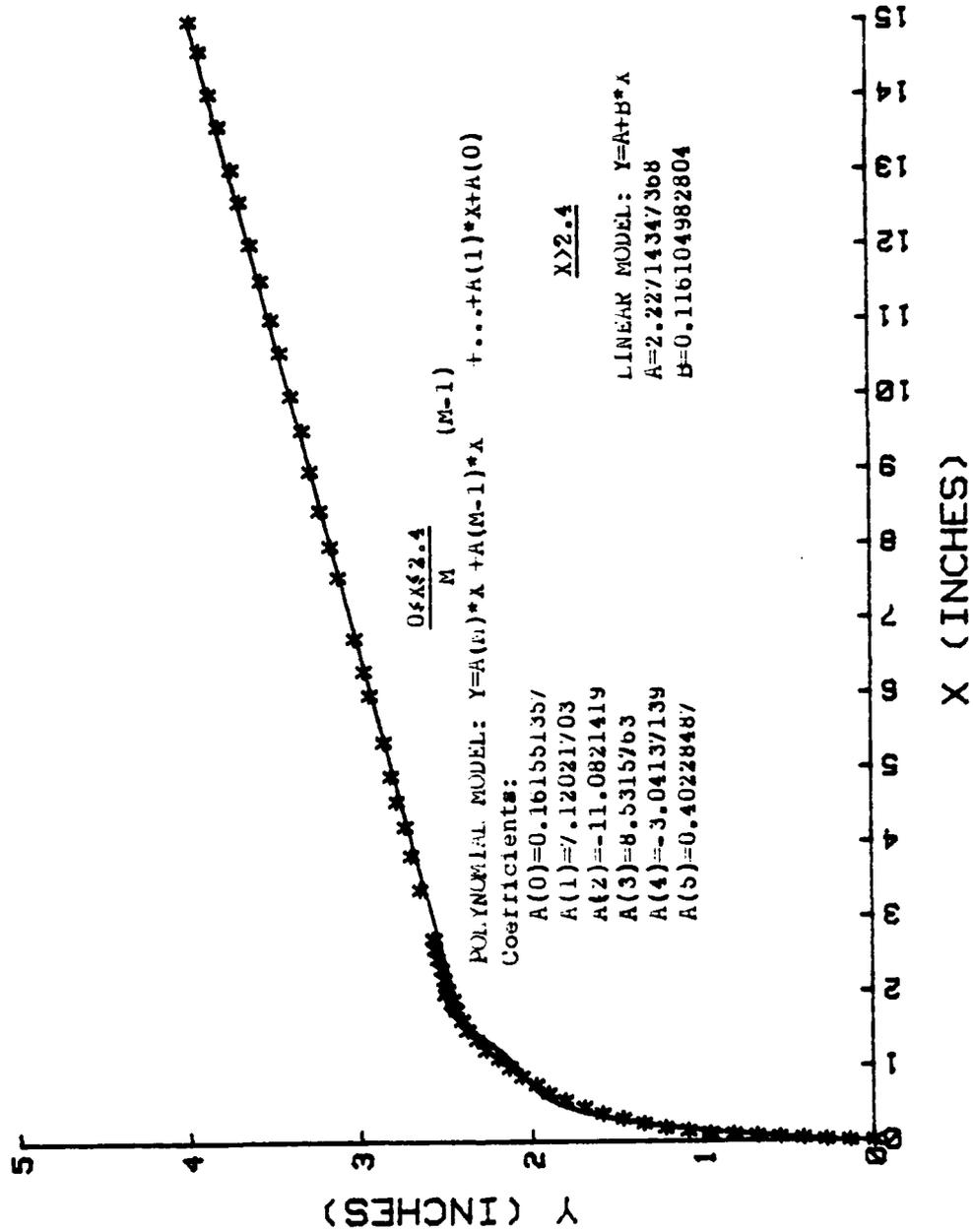
Figure A-1. Nose Shape at 250,000 Feet

$0 \leq X \leq 2.4$

POLYNOMIAL MODEL: $Y=A(M)*X^M +A(M-1)*X^{(M-1)} +...+A(1)*X+A(0)$

Coefficients:

A(0)=0.196395569
A(1)=5.76313298
A(2)=-7.5019411
A(3)=4.925666
A(4)=-1.51496709
A(5)=0.17410385

$X > 2.4$

LINEAR MODEL: $Y=A+B*X$

A=2.22714347368
B=-0.116104982804

X (INCHES)

Y (INCHES)
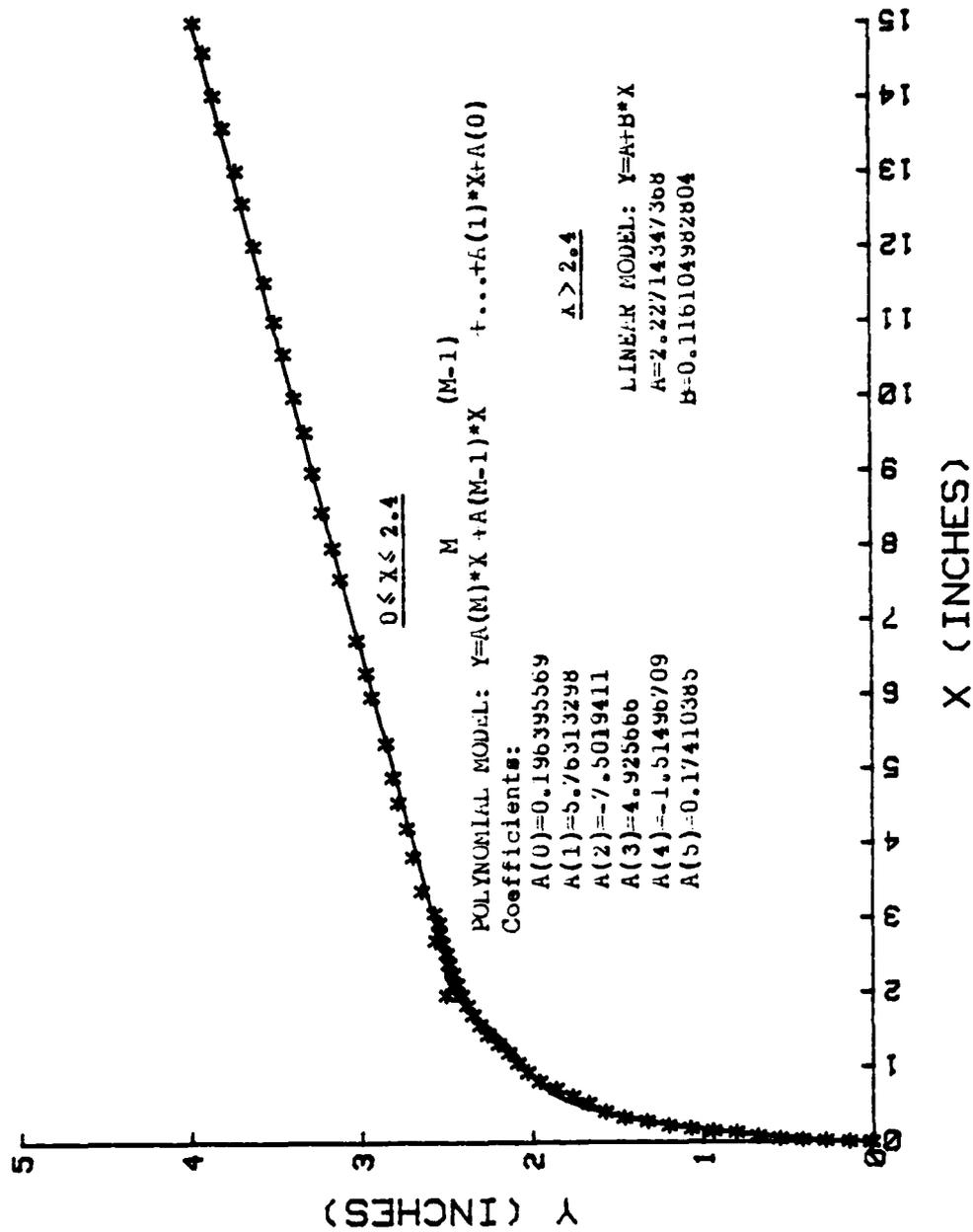
Figure A-2. Nose Shape at 90,000 Feet

POLYNOMIAL MODEL: $Y=A(M)*X^M +A(M-1)*X^{(M-1)} +...+A(1)*X+A(0)$

$0 \leq X \leq 2.4$

$X > 2.4$

Coefficients:

A(0)=0.0286729/3
A(1)=4.33219529
A(2)=-4.5429413
A(3)=2.7045/9
A(4)=-0.77793/931
A(5)=-0.084166199

LINEAR MODEL: $Y=A+B*X$
A=2.192069//312
B=0.112/8195b692

X (INCHES)

Y (INCHES)
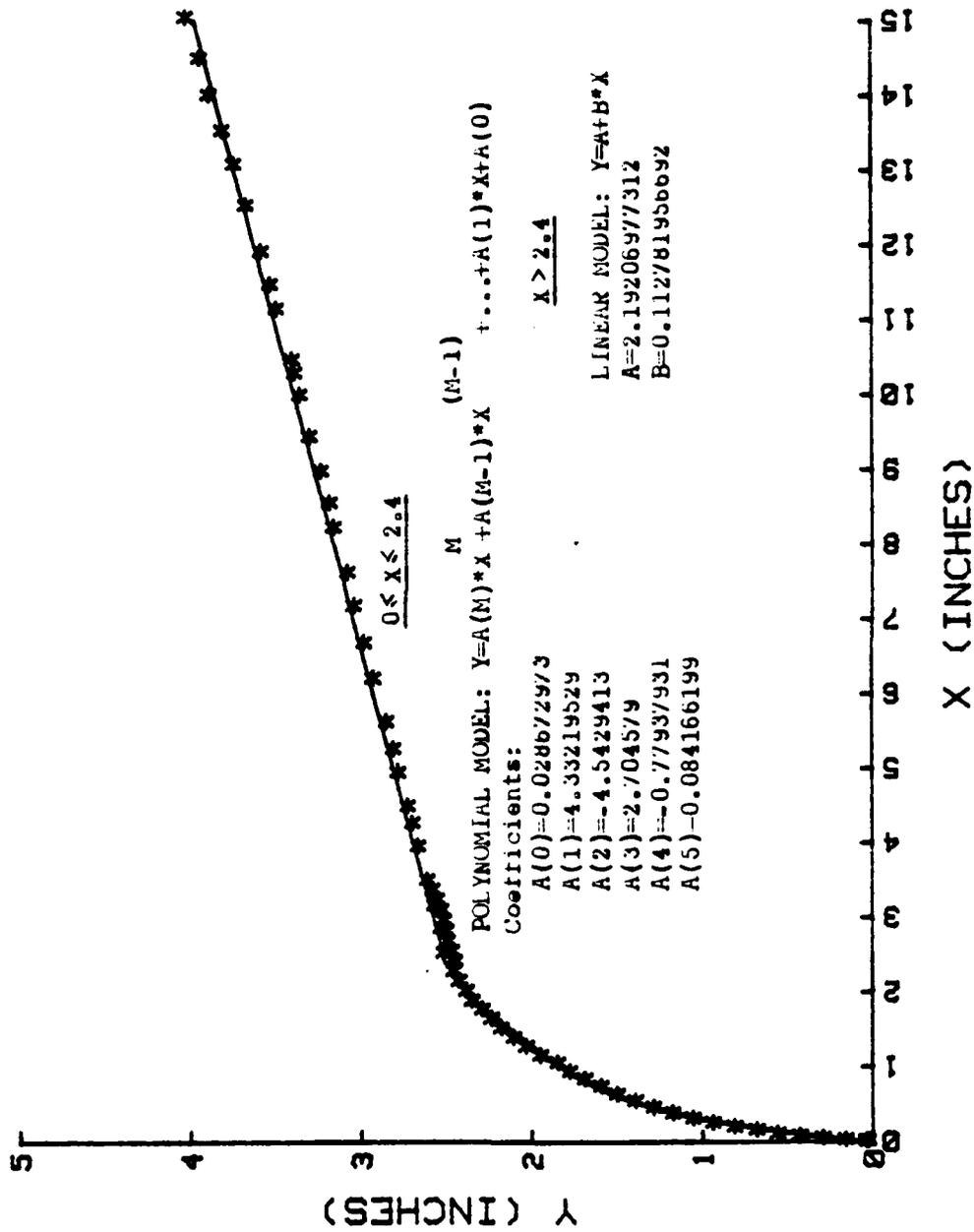
Figure A-3. Nose Shape at 56,250 Feet

74

$0 < X < 2.4$

POLYNOMIAL MODEL: $Y = A(M) \cdot X^M + A(M-1) \cdot X^{(M-1)} + \ldots + A(1) \cdot X + A(0)$

Coefficients:
A(0)=0.04745/311
A(1)=3.353227/24
A(2)=-6.313494
A(3)=5.913/079
A(4)=-2.23930/68
A(5)=0.293023988

$X > 2.4$

LINEAR MODEL: $Y = A + B \cdot X$
A=2.232680897b
B=0.11bb2090759b

X (INCHES)

Y (INCHES)

5   4   3   2   1   0

0 1 2 3 4 5 6 7 8 9 10 11 12 13 14 15
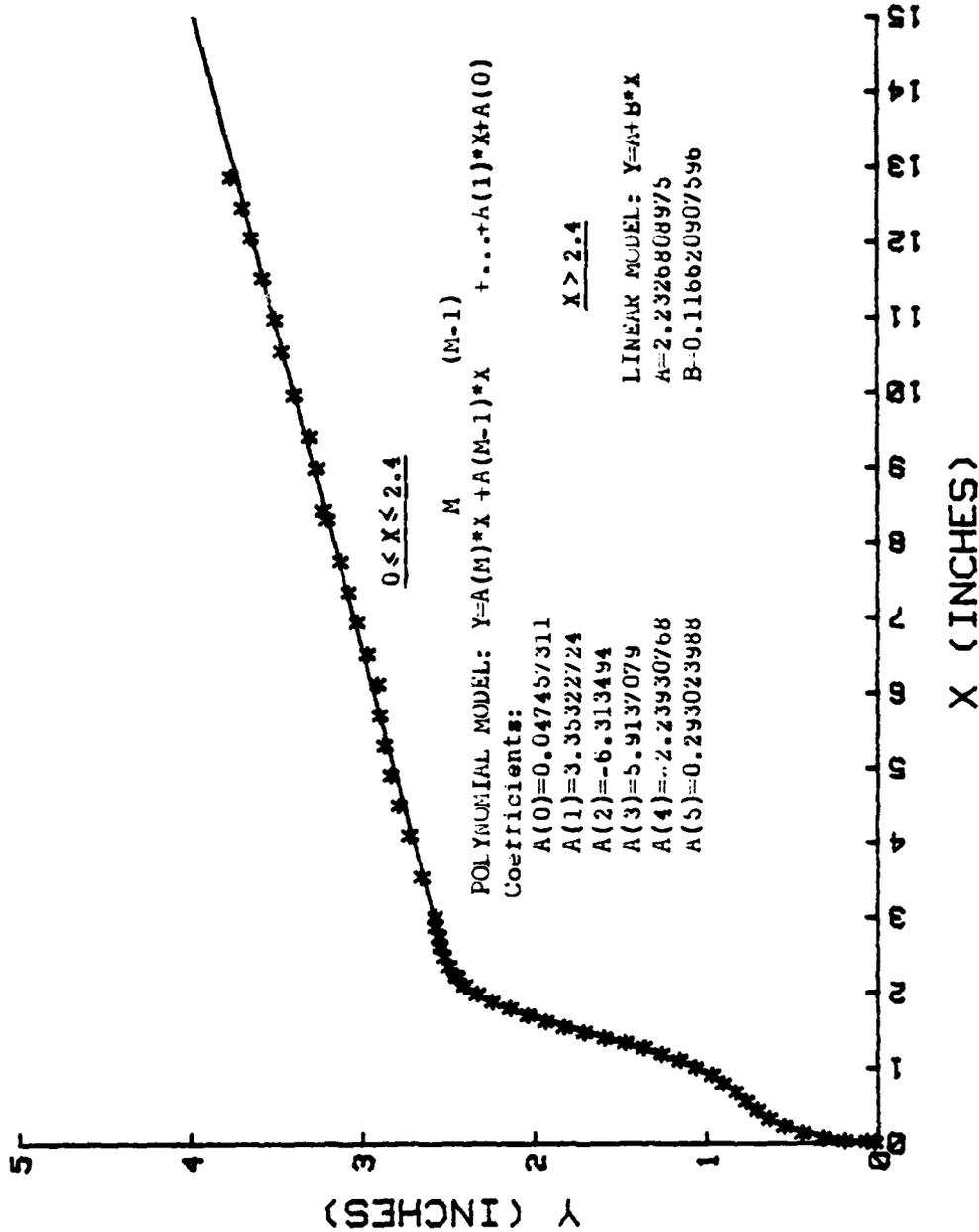
Figure A-4. Nose Shape at 40,100 Feet

POLYNOMIAL MODEL: $Y=A(M)*X^{M}+A(M-1)*X^{(M-1)}+...+A(1)*X+A(0)$

$0 \leq X \leq 2.4$

Coefficients:
A(0)=-0.0416525554
A(1)=-3.4907407?
A(2)=8.4911811
A(3)=9.1455531
A(4)=-3.818640b
A(5)=-0.5454302

$X > 2.4$

LINEAR MODEL: $Y=A+B*X$
A=2.1943b624b2b
B=0.1752816397?5

X (INCHES)

Y (INCHES)
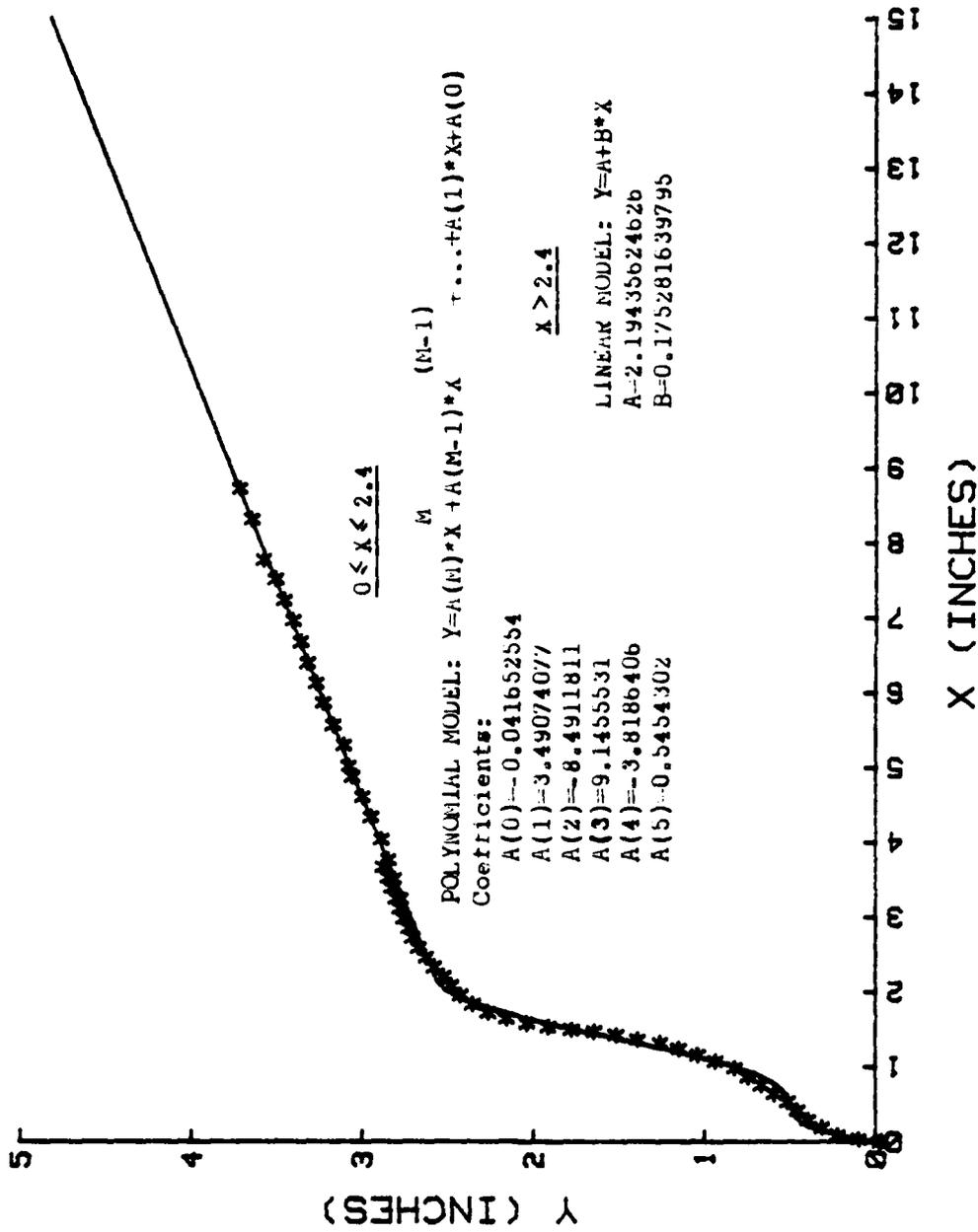
Figure A-5. Nose Shape at 25,000 Feet

76
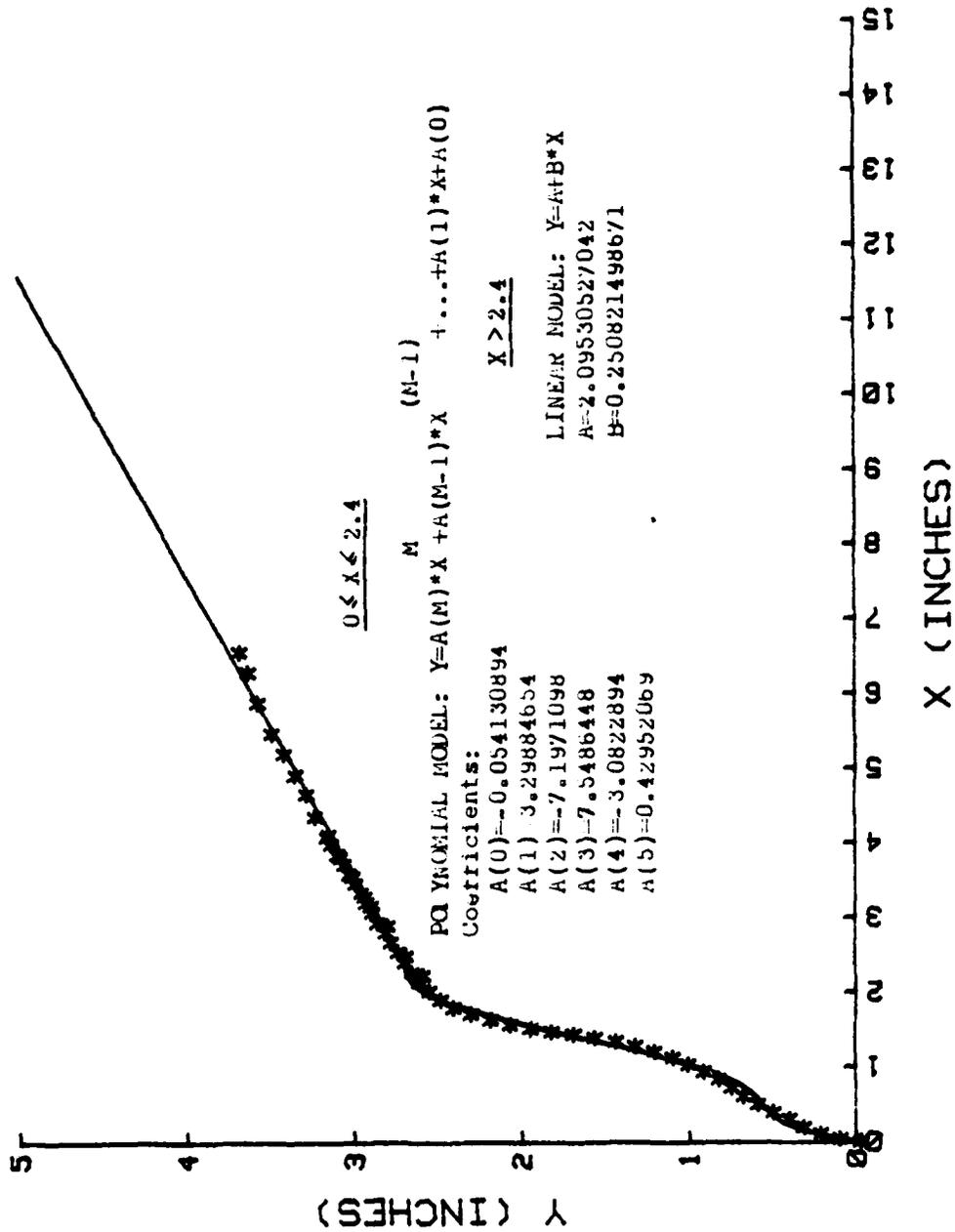
Figure A-6. Nose Shape at 15,500 Feet

APPENDIX B
POLYNOMIAL REPRESENTATION OF COEFFICIENTS

The following pages contain graphs of the various nose shape coefficients defined in equations (49) through (52). The first six graphs correspond to the coefficients used in equations (49) and (51) and apply for $0 \leq x \leq 2.4$ inches where x is centerline distance from the nose tip. The last two graphs correspond to coefficients used in equations (50) and (52) and apply for $x > 2.4$ inches.

ALTITUDE ≤ 90,000 Ft

POLYNOMIAL MODEL: $Y=A(M)*X^M +A(M-1)*X^{(M-1)} +...+A(1)*X+A(0)$

Coefficients:
A(0)=-2.07654584
A(1)=0.000299595219
A(2)=-1.18033974E-08
A(3)=-2.0437866E-13
A(4)=1.6226952JE-18
A(5)=4.8592335BE-24

ALTITUDE > 90,000 Ft

LINEAR MODEL: $Y=A+B*X$
A=0.051046278755
B=1.39107853462E-06

Figure B-1. Graph of Coefficient A(5) versus Altitude

79

ALTITUDE ≤ 90,000 ft

POLYNOMIAL MODEL: $Y=A(M)*X^{M}+A(M-1)*X^{(M-1)}+...+A(1)*X+A(0)$

Coefficients:

A(0)=8.3422562
A(1)=-0.0013492108B
A(2)=5.2480564E-08
A(3)=-8.6233637E-13
A(4)=6.4052595E-18
A(5)=-1.7798141E-23

ALTITUDE >90,000 ft

LINEAR MODEL: $Y=A+B*X$

A=-0.5990936922
B=-9.6999814236bE-06

ALTITUDE (FEET)

A(4)

25000 50000 75000 100000 125000 150000 175000 200000 225000 250000

0 -1 -2 -3 -4
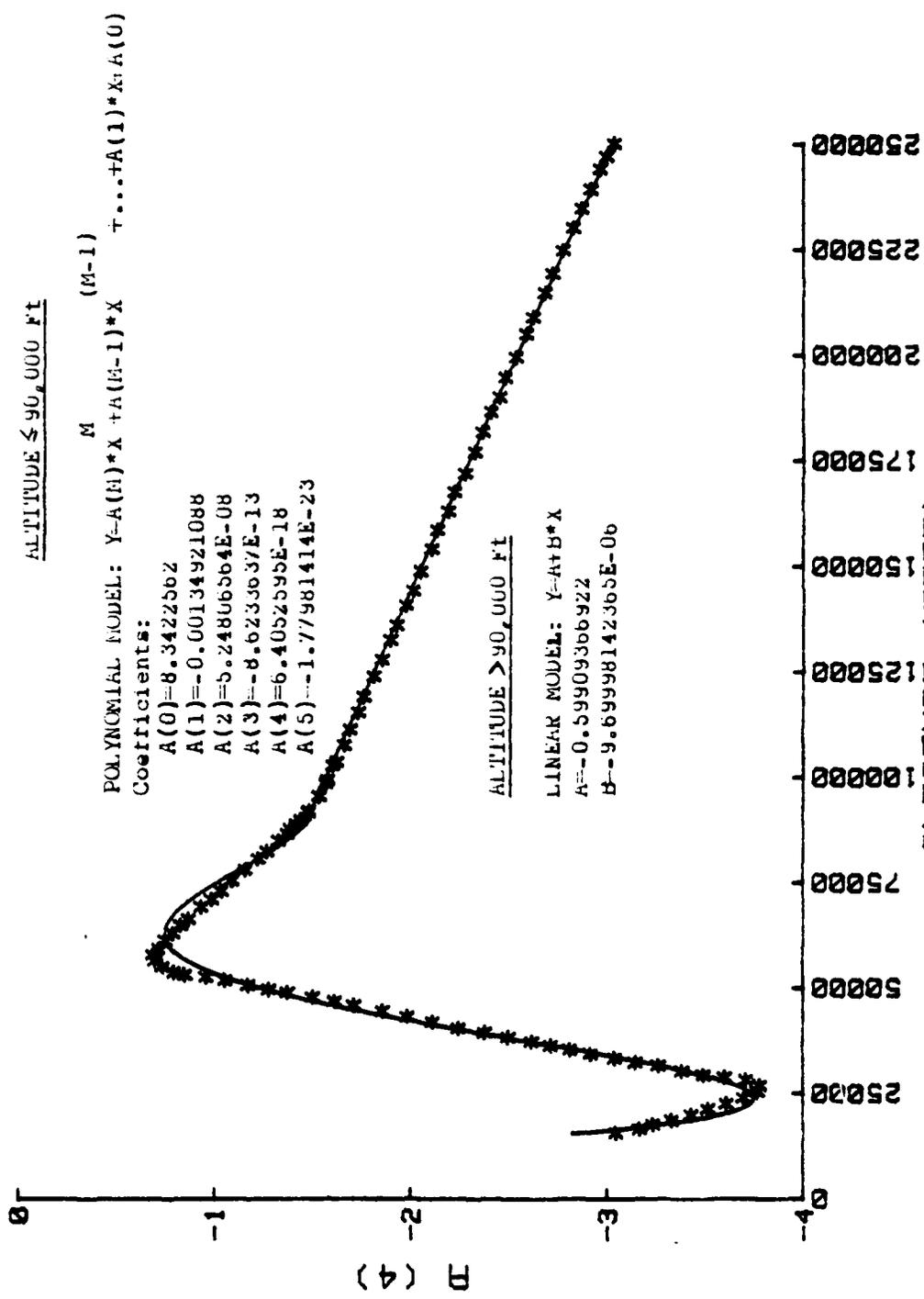
Figure B-2. Graph of Coefficient A(4) versus Altitude

ALTITUDE ≤ 90,000 ft

POLYNOMIAL MODEL: $Y=A(M)*X^m + A(M-1)*X^{(M-1)} \ldots + A(1)*X + A(0)$

Coefficients:

A(0)=-14.5288361
A(1)=0.00254/135b
A(2)=-9.2o/848E-08
A(3)=1.33/4005E-12
A(4)=-7.7b019/E-18
A(5)=1.2b888/3E-23

ALTITUDE > 90,000 ft

LINEAR MODEL: $Y=A+B*X$

A=-2.9353885087
B=-2.2b/07b28322E-05

B (3)
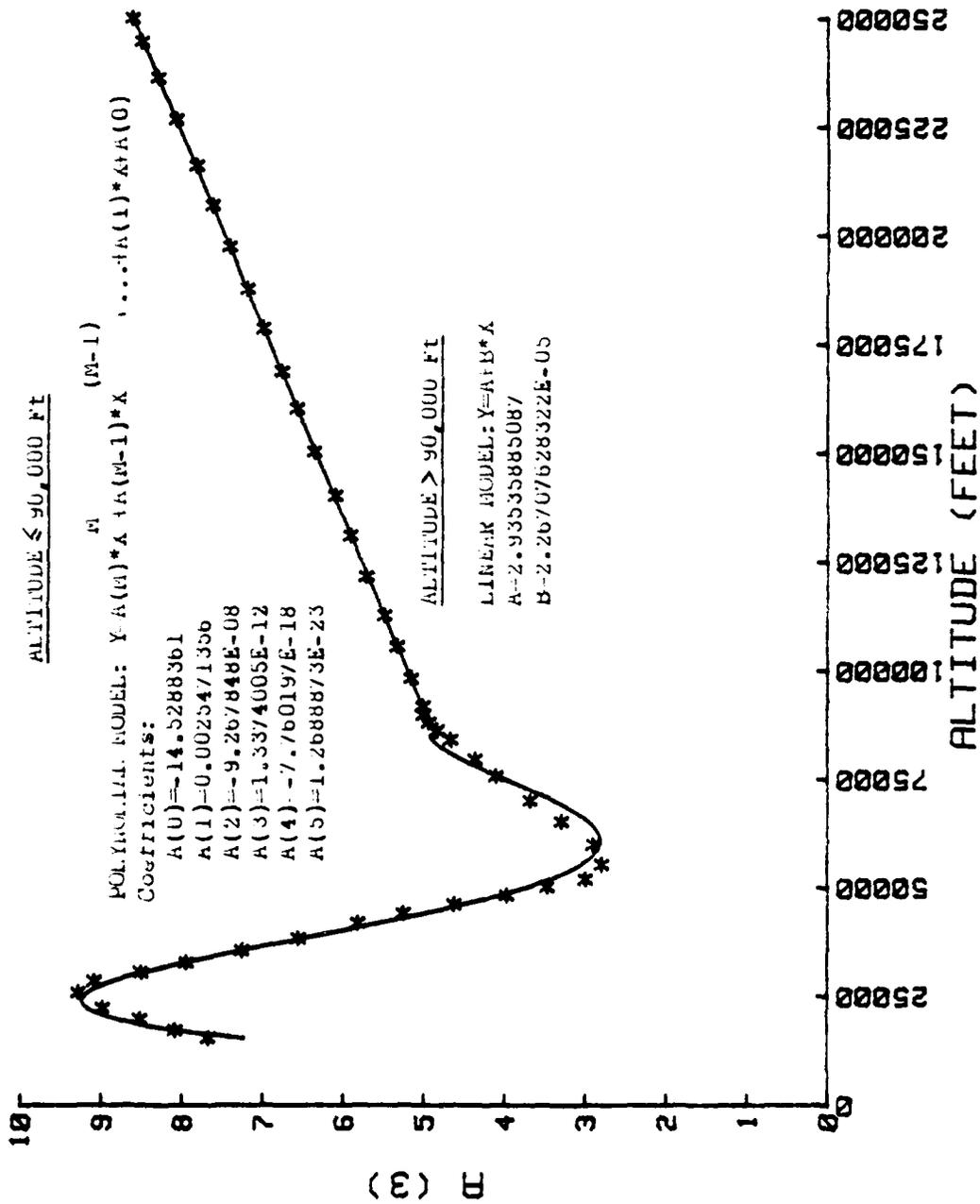
ALTITUDE (FEET)

Figure B-3. Graph of Coefficient A(3) versus Altitude

ALTITUDE ≤ 90,000 Ft

POLYNOMIAL MODEL: $Y = A(M)*X^M + A(M-1)*X^{(M-1)} + \ldots + A(1)*X + A(0)$

Coefficients:

A(0)=-13.858879
A(1)=-0.0024723682
A(2)=9.7400192-08
A(3)=-1.6430241E-12
A(4)=1.2418752E-17
A(5)=-3.4660006E-23

ALTITUDE > 90,000 Ft

LINEAR MODEL: $Y = A + B*X$
A=-5.4663295447
B=-2.218811/88/2E-05

A (2)
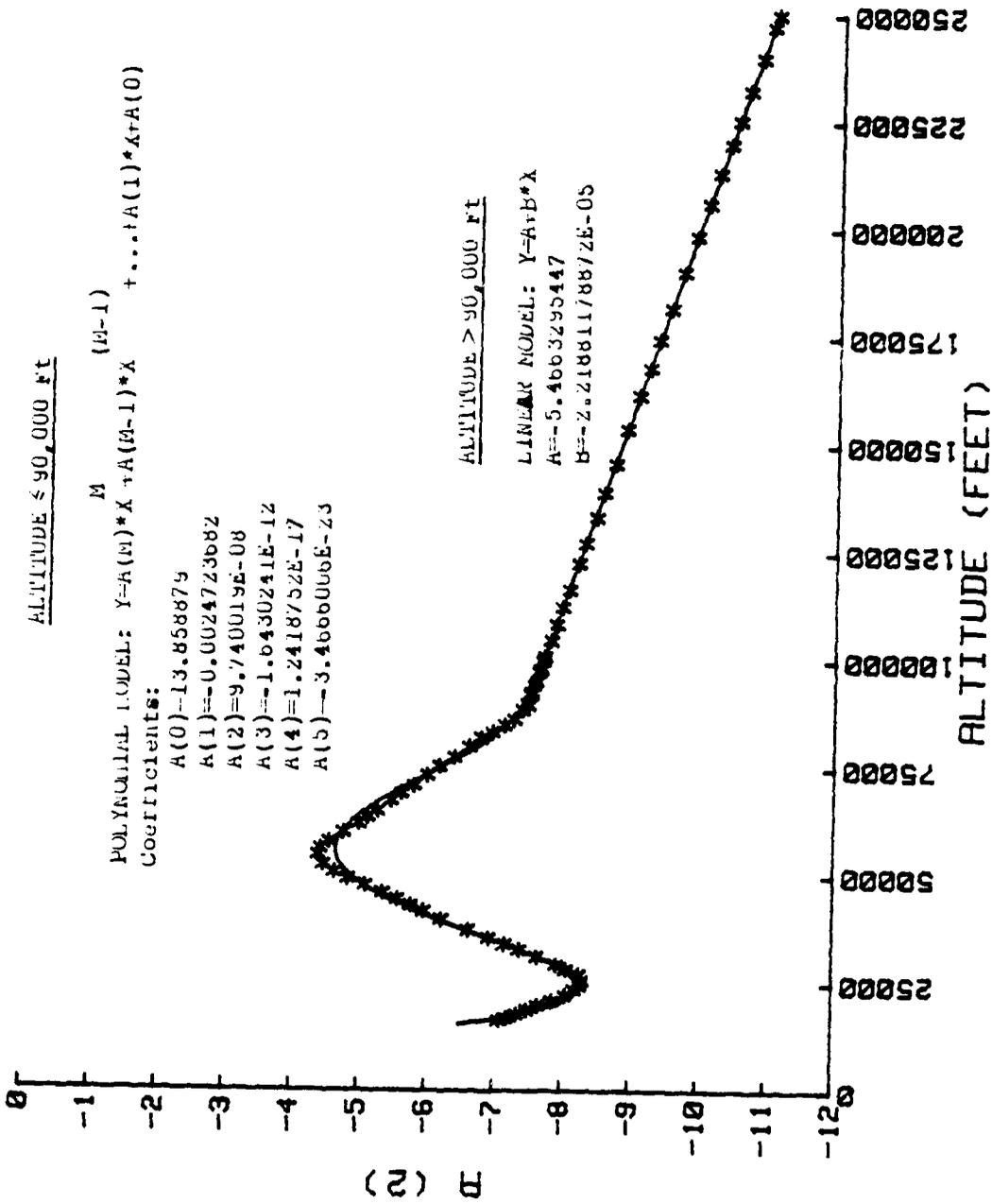
ALTITUDE (FEET)

Figure B-4. Graph of Coefficient A(2) versus Altitude

82

ALTITUDE ≤ 90,000 Ft

POLYNOMIAL MODEL: $Y = A(N)*X^M + A(M-1)*X^{(M-1)} + \ldots + A(1)*X + A(0)$

Coefficients:

A(0)=-2.243164   A(5)=-1.060971E-22
A(1)=-0.0008225887   A(6)=-2.824389E-28
A(2)=-4.484564E-08
A(3)=-1.179345E-12
A(4)=-1.583495E-17

ALTITUDE > 90,000 Ft

LINEAR MODEL: $Y = A + B*X$
A=5.049703804412
B=8.120712993E-06
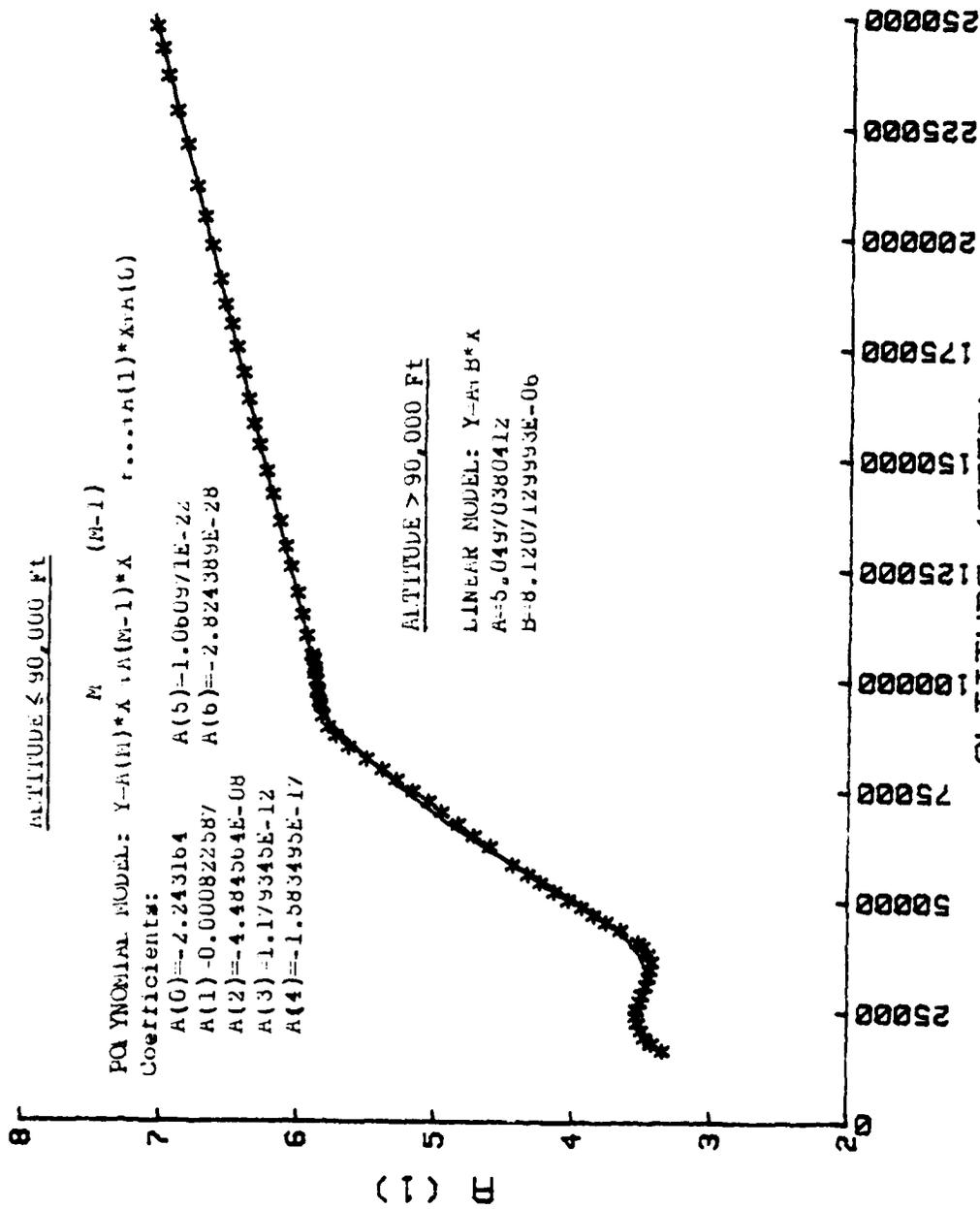
ALTITUDE (FEET)

Figure B-5. Graph of Coefficient A(1) versus Altitude

83

ALTITUDE (FEET)

A (0)

ALTITUDE ≤ 90,000 ft

POLYNOMIAL MODEL: $Y = A(M) * X^{(M-1)} + \ldots + A(1)*X + A(0)$

Coefficients:
A(0)=-1.4477393
A(1)=-0.0002283692/
A(2)=1.2936294E-08
A(3)=-3.501036E-13
A(4)=4.902432E-18
A(5)=-3.4147616-23
A(6)=-9.3577516-29

ALTITUDE > 90,000 ft

LINEAR MODEL: $Y = A.B*X$
A-0.214283168408
B=-2.012908835bE-07
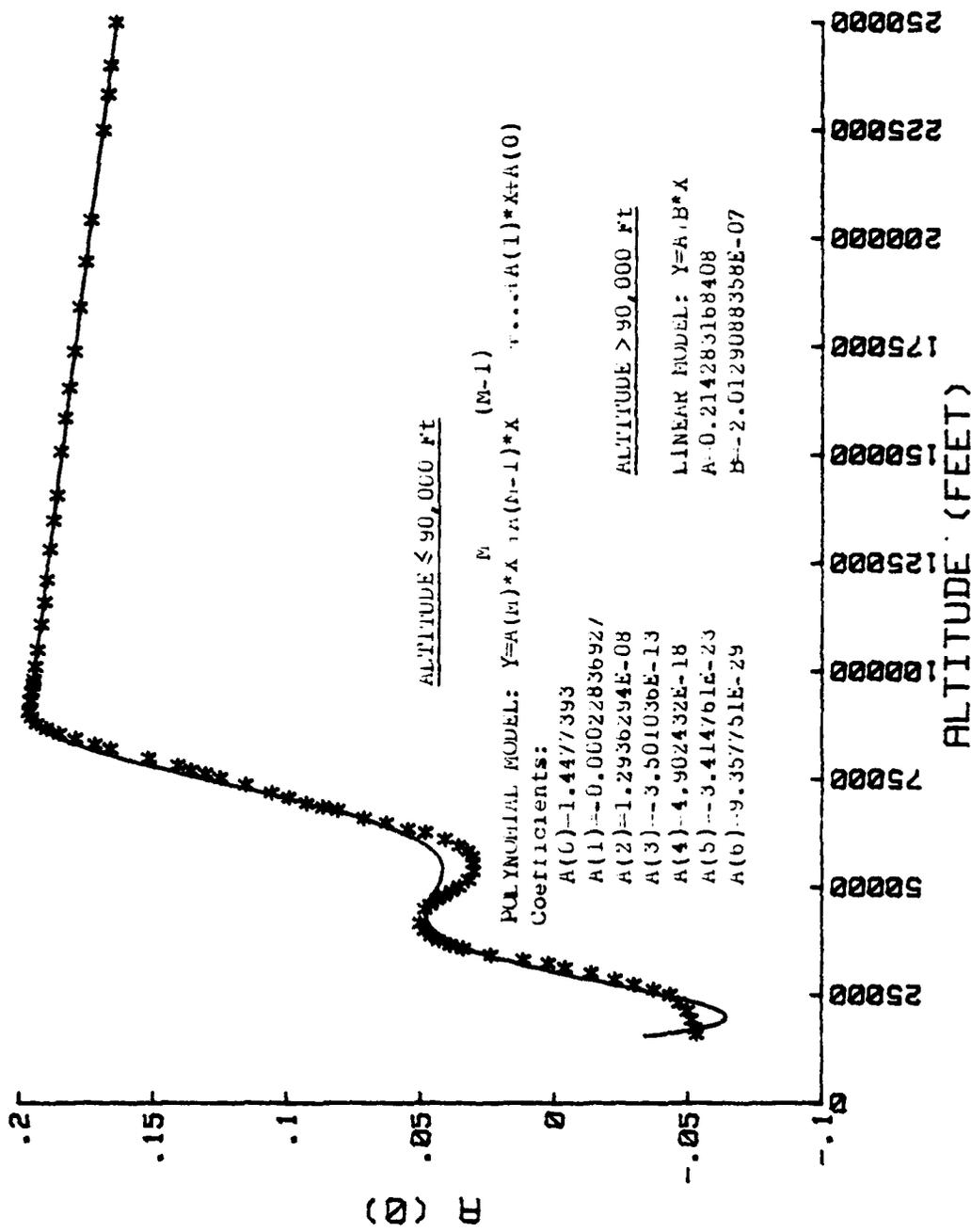
Figure B-6. Graph of Coefficient A(0) versus Altitude

ALTITUDE ≤ 90,000 Ft

POLYNOMIAL MODEL: $Y = A(M)*X^{(M-1)} + A(M-1)*X^{(M-1)} + \ldots + A(1)*X + A(0)$

Coefficients:
A(0)=1.6357927
A(1)=-0.00002892953
A(2)=-4.9067gE-10
A(3)=-2.77394E-15
A(4)=-6.1321E-21
A(5)=-7.7654lE-26

ALTITUDE > 90,000 Ft

LINEAR MODEL: $Y = A + B*X$
A=2.2318534b02b
B=-1.84b9b773b04E-09

ALTITUDE (FEET) versus Altitude
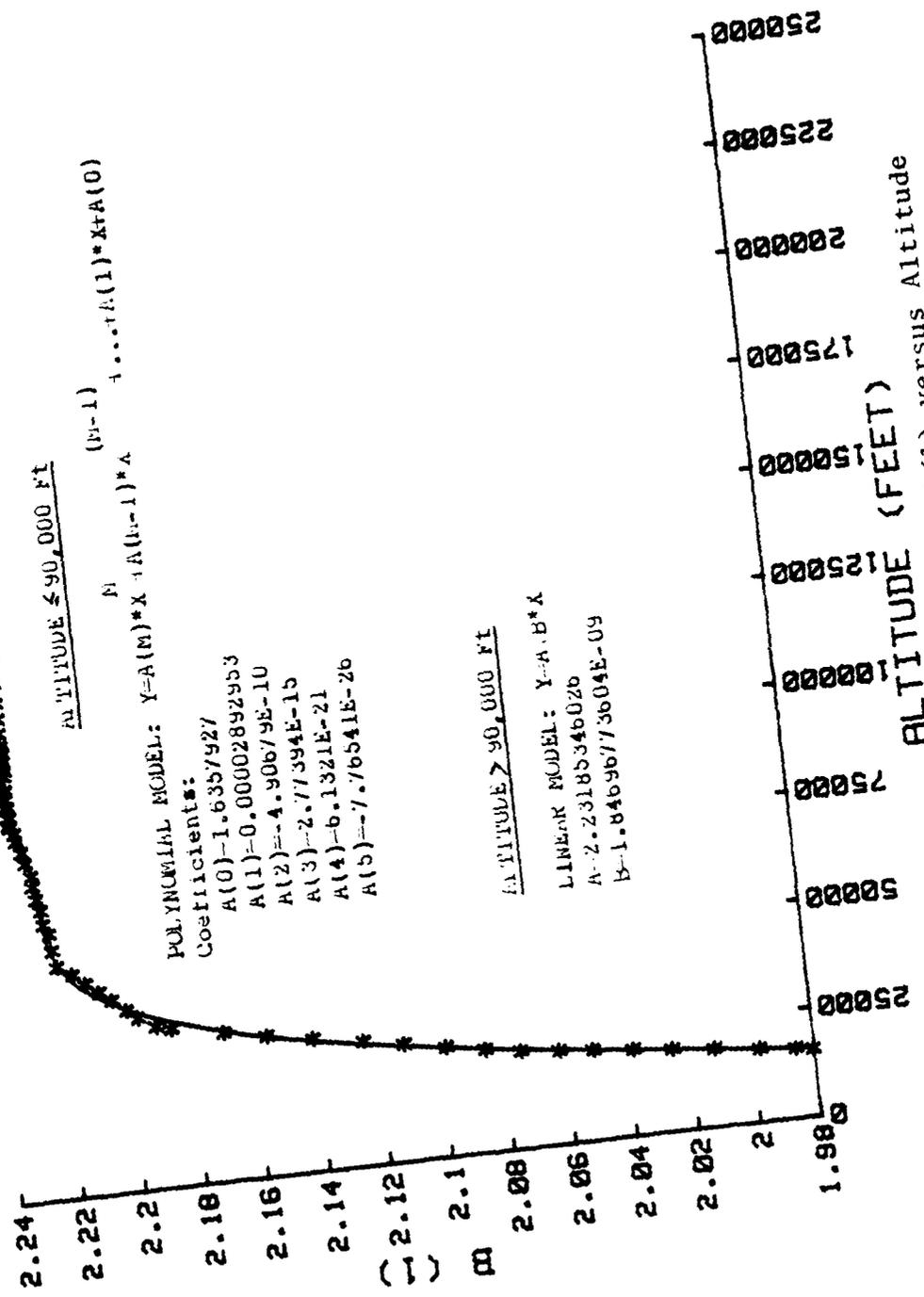
Figure B-7. Graph of Coefficient B(1) versus Altitude

ALTITUDE ≤ 90,000 ft

POLYNOMIAL MODEL: $Y = A(M)*X^{(M-1)} + A(M-1)*X^{(M-1)} + ... + A(1)*X + A(0)$

Coefficients:

A(0)=0.14741578
A(1)=0.000141859
A(2)=-9.258142E-10
A(3)=-2.251935E-14
A(4)=-2.64915bE-19
A(5)=-1.51bb51E-24
A(b)=-3.38b093E-30

ALTITUDE > 90,000 ft

LINEAR MODEL: $Y = A + B*X$

A=0.11b0700727373737
B=-2.333100b0221E-09

B (0)

ALTITUDE (FEET)

Figure B-8. Graph of Coefficient B(0) versus Altitude

APPENDIX C

POLYNOMIAL REPRESENTATION OF NOSE TIP RECESSION

The following graph shows the evaluation of nose tip recession, the distance the nose tip ablates from the original location, as shown in Figure 10. As for the coefficients described in Appendix B, the nose tip recession was divided into two portions. A sixth-order polynomial describes the nose tip recession below 90,000 feet and a linear model describes the recession above 90,000 feet.
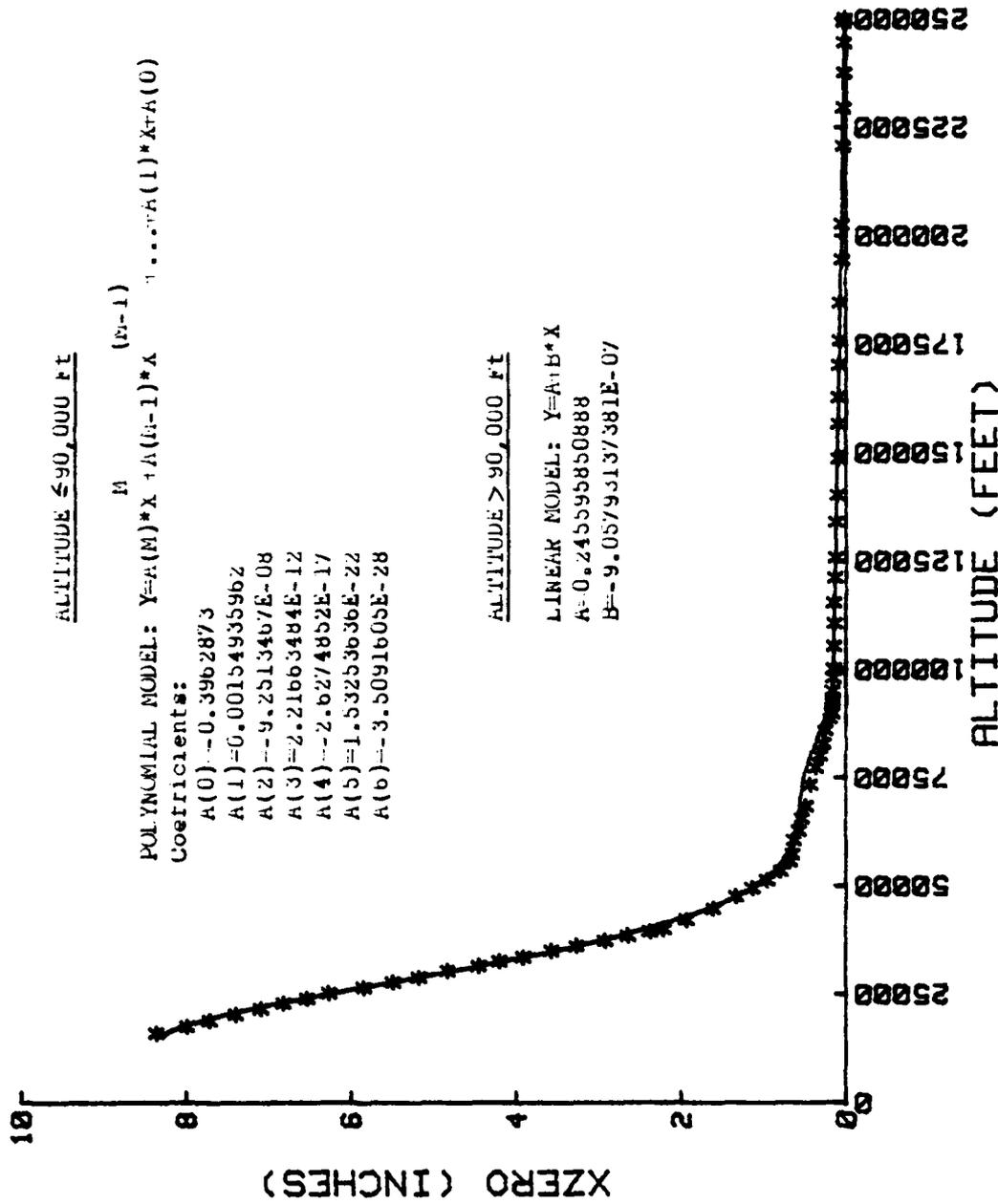
Figure C-1. Graph of Coefficient XZERO versus Altitude

APPENDIX D

COMPUTER PROGRAM EXAMPLE

Appendix D is a sample of the computer program used to conduct the trajectory analysis. The computations were conducted on an HP-9845A computer which uses BASIC computer language. In general, the program is self-explanatory in that the names of variables are used whenever possible.

Line numbers beginning with 1XXX describe the initial conditions. The counter K is zero until zero altitude is reached and then is equal to one. The counter L is zero during the first iteration and allows the establishment of initial volume, mass, and base area of the reentry body. After the first iteration of nose shape, L is equal to 1. The counter Z is zero until the altitude of the cloud is reached. The value of Z is changed to one during the iteration to find the mass loss due to the impact of the ice in the cloud. After the iteration is complete, the value of Z is two. If Z is set equal to two initially, the baseline trajectory with no ice ablation will be calculated.

Line numbers beginning with 2XXX calculate the new position of the body as it descends. Line numbers beginning with 4XXX calculate all of the major parameters needed for the calculation of pressure coefficients and the nose shape coefficients. Line numbers beginning with 5XXX calculate the actual nose shape, pressure coefficient, drag, volume,

etc. Line numbers beginning with 6XXX calculate the initial volume, mass and base area and values of drag coefficient and ballistic coefficient during the entire reentry. Line numbers beginning with 7XXX print the final values obtained during reentry and stop the program. Line numbers beginning with 8XXX calculate the mass ablated during passage through the ice cloud. Line numbers beginning with 9XXX calculate the final range and set the final altitude to zero so that calculation of other parameters at zero altitude is possible.

TRAJECTORY WITH ICE ABLATION

```
1       ! THIS PROGRAM CALCULATES THE TRAJECTORY OF A HYPERSONIC REENTRY
        !   VEHICLE USING NEWTONIAN FLOW.!
2       ! IT CALCULATES THE DRAG, CHANGE IN MASS, MACH NUMBER AND TRAJECTORY
        !   AS FUNCTIONS OF EXPERIMENTALLY DETERMINED NOSE SHAPE VS ALTITUDE!
3       ! THE PORTION OF THE PROGRAM FROM 1000 TO 3000 ALLOWS FOR THE INPUT OF
        !   INITIAL VALUES AND FOR THE CALCULATION OF THE ACTUAL TRAJECTORY.!
4       ! INPUT VALUES OF INITIAL X AND Y DISPLACEMENT IN XINITIAL AND YINITIAL
        !   RESPECTIVELY.
5       ! INPUT INITIAL VALUE OF REENTRY ANGLE IN AINITIAL. NOTE: FOR REENTRY
        !   AINITIAL MUST BE NEGATIVE.
6       ! **************************************************************
1000    K=0
1001    L=0
1002    N=4
1004    Z=0                                 !IF Z=0 THEN ICE ABLATION  IS  IN-
                                            !   INCLUDED. OTHERWISE Z=2.
1005    Cloud_density=.24*.3048^3/(454*32.2) !THE FIRST NUMBER IS G/M3...THE
                                            !   OTHERS CONVERT TO SLUG/FT3
1006    Cloud_thickness=5000                !FEET
1007    Cloud_altitude=30000                !FEET
1008    Delta_h=0                           !VARIABLE WHICH PROVIDES ALTITUDE
                                            !   OFFSET FOR IMPACT ABLATION
1009    Mass_factor=10                      !#GRAMS ABLATED/GRAM OF ICE
1010    G=32.2                              !FEET/SEC
1020    Dtime=.1                            !SECONDS
1030    Totime=0                            !SECONDS
1040    Vinitial=21632                      !FT/SEC
```

91

TRAJECTORY WITH ICE ABLATION

```
1050   Ainitial=-25.0*PI/180           !FIRST NUMBER IN DEGREES....CONVERTS
                                        TO RADIANS
1060   Yinitial=250000                 !FEET
1070   Xinitial=0                      !FEET
1080   V=Vinitial*SIN(Ainitial)        !FT/SEC
1090   U=Vinitial*COS(Ainitial)        !FT/SEC
1100   Gamma=1.4
1101   DIM A(6),B(8,2),C(9,7)
1102   FOR I=1 TO 8
1103   FOR J=1 TO 2
1104   READ B(I,J)
1105   NEXT J
1106   NEXT I
1107   FOR I=1 TO 9
1108   FOR J=1 TO 7
1109   READ C(I,J)
1110   NEXT J
1111   NEXT I
1113   DATA .2142831634O3,-2.0129083358OE-07,5.0497030380412,8.1207129993E-06,-5.46
63295447,-2.2188117387272E-05,2.9353585085087,2.2670762832E-05,-.5990936692922
1114   DATA -9.699981423265E-06,.051046278755,1.3910785346E-06,2.2318534026,.116
070072737,.245595850888,-9.05793137381E-07
1115   DATA 1.4477393,-.00022836927,1.2936294E-08,-3.50103E-13,4.902432E-18,-3.4
14761E-23,9.3577751E-29
1116   DATA -2.243164,.000082225E7,-4.484564E-08,1.179345E-12,-1.583495E-17,1.06097
1E-22,-2.824389E-28
1117   DATA 13.858879,-.0024723682,9.740019E-08,-1.6430241E-12,1.2418752E-17,-3.4
66600GE-23,0
```

TRAJECTORY WITH ICE RELATION

```
1118  DATA -14.5288361,.0025471356,-9.267848E-08,1.3374005E-12,-7.760197E-18,1.2
688873E-23,0
1119  DATA 8.3422562,-.0013492108B,5.2480656⁴E-08,-8.6236637E-13,6.4052595E-18,-
1.77981414E-23,0
1120  DATA -2.07654584,.0002959995219,-1.1803374E-08,2.04378666E-13,-1.62269523E-
18,4.85923358E-24,0
1121  DATA .14741578,.00001141859,-9.258142E-10,2.251935E-14,-2.649156E-19,1.5166
51E-24,-3.386093E-30
1122  DATA 1.6357827,.00002892953,-4.90679E-10,2.77394E-15,6.1321E-21,-7.76541E-
26,0
1123  DATA -.3962873,.001549035962,-9.2513467E-08,2.21663484E-12,-2.6274852E-17,1
.53253636E-22,-3.5091605E-28
1140  Rhomissile=2.2*62.4/(32.2*12^3)
1150  Mach_no=Vinitial/973.4
1160  PRINT "Y INITIAL=",Yinitial,"FT"
1161  PRINT "X INITIAL=",Xinitial,"FT"
1162  PRINT "INITIAL VELOCITY =",Vinitial,"FT/SEC"
1163  PRINT "MACH NO=",Mach_no
1164  PRINT "INITIAL ENTRY ANGLE=",Ainitial,"RADIANS"
1165  PRINT
1166  PRINT
1170  Y2=Yinitial+V*Dtime
1180  X2=Xinitial+U*Dtime
1181  Y2_modified=Y2
1190  GOTO 4000
1191  ! *******************************************************
1192  !
```

93

```
1193  ! THE FOLLOWING SECTION CALCULATES THE TRAJECTORY
2000  Xaccel=-Total_drag*COS(Ainitial)/(Tmass-Dmass)
2001  Yaccel=-G-Total_drag*SIN(Ainitial)/(Tmass-Dmass)
2005  X3=Xaccel*Dtime^2+2*X2-Xinitial
2010  Y3=Yaccel*Dtime^2+Y2*2-Yinitial
2020  Totime=Totime+Dtime
2030  Ainitial=ATN((Y3-Y2)/(X3-X2))
2040  V=(Y3-Y2)/Dtime
2050  U=(X3-X2)/Dtime
2060  IF Y3<=0 THEN 9000
2070  Xinitial=X2
2080  Yinitial=Y2
2090  Y2=Y3
2100  X2=X3
2105  Y2_modified=Y2+Delta_h
2110  GOTO 4000
4000  V1=SQR(V^2+U^2)
4010  Rho=.0027*EXP(-Y2/23500)
4020  Total_drag=0
4030  Q=.5*Rho*V1^2
4040  IF Y2<35000 THEN 4200
4050  Temp=393
4060  GOTO 4300
4200  Temp=519-Y2/280
4300  Vsound=49.1*SQR(Temp)
4310  Mach_no=V1/Vsound
```

94

TRAJECTORY WITH ICE ABLATION

```
4320   IF Mach_no<=5 THEN 4330
4330   P1=((Gamma+1)/2*Mach_no^2)^(Gamma/(Gamma-1))
4340   P2=((Gamma+1)/(2*Gamma*Mach_no^2-Gamma+1))^(1/(Gamma-1))
4350   Cpo=2/(Gamma*Mach_no^2)*(P1*P2-1)
4360   Xnose=0
4370   Ynose=0
4380   IF Y2_modified<15000 THEN 5000
4390   IF Y2<90000 THEN 4500
4391   Xzero=B(8,1)+B(8,2)*Y2_modified      !CALCULATING THE NOSE COEFFICIENTS FOR
                                             ALTITUDE GREATER THAN 90000 FEET.
4400   IF Xzero<0 THEN Xzero=0
4401   Aa=B(7,1)
4402   Bb=B(7,2)
4403   FOR I=1 TO 6
4404   A(I)=B(I,1)+B(I,2)*Y2_modified
4405   NEXT I
4410   GOTO 5000
4500   Xzero=0
4510   FOR J=1 TO 7                         !CALCULATING THE NOSE COEFFICIENTS FOR ALTITUDE
                                             BETWEEN 15000 AND 90000 FEET
4520   Xzero=Xzero+C(9,J)*Y2_modified^(J-1)
4530   NEXT J
4540   Aa=0
4550   FOR J=1 TO 7
4560   Aa=Aa+C(8,J)*Y2_modified^(J-1)
4570   NEXT J
4580   Bb=0
```

95

AD-A098 474   NAVAL POSTGRADUATE SCHOOL MONTEREY CA   F/G 12/1
                A COMPUTER STUDY OF THE EFFECT OF ICE CLOUDS ON THE CEP OF A ZE--ETC(U)
   DEC 80   M W MELLOR

UNCLASSIFIED   NL

END
DATE
FILMED
8-81
DTIC
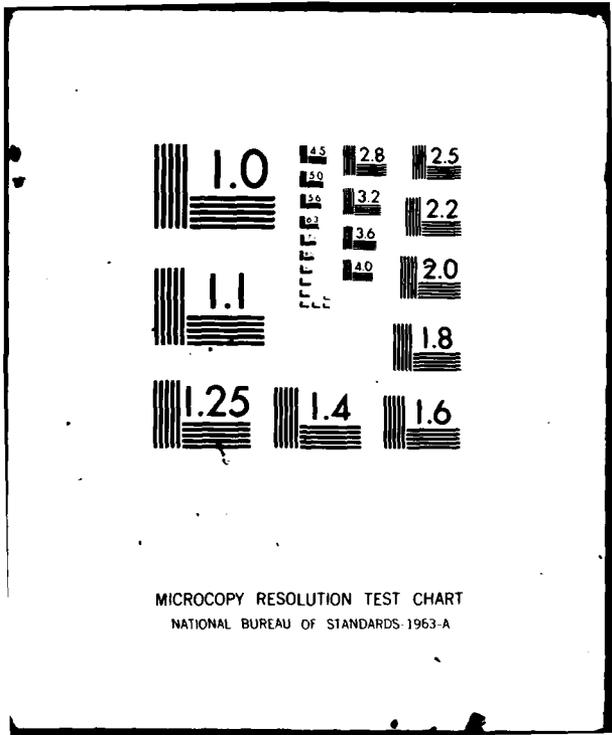
MICROCOPY RESOLUTION TEST CHART
NATIONAL BUREAU OF STANDARDS-1963-A

TRAJECTORY WITH ICE ABLATION

```
4590    FOR J=1 TO 7
4600    Bb=Bb+C(7,J)*Y2_modified^(J-1)
4610    NEXT J
4620    FOR I=1 TO 6
4630    A(I)=0
4640    FOR J=1 TO 7
4650    A(I)=A(I)+C(I,J)*Y2_modified^(J-1)
4660    NEXT J
4670    NEXT I
4680    GOTO 5000
5000    Xnose=Xzero
5001    Volume=0                           !THIS SECTION CALCULATES NOSE SHAPE
5002    F=1
5003    X2nose=Xnose+.1*F
5004    IF X2nose>=60 THEN X2nose=60
5005    Xprime=X2nose-Xzero
5007    IF X2nose>=20 THEN Y2nose=B(7,1)+B(7,2)*X2nose
5008    IF X2nose>=20 THEN 5041
5010    IF Xprime>=2.4 THEN 5040
5020    Y2nose=A(6)*Xprime^5+A(5)*Xprime^4+A(4)*Xprime^3+A(3)*Xprime^2+A(2)*Xprime
+A(1)
5021    Y3nose=Aa+Bb*Xprime
5022    IF Y3nose<Y2nose THEN Y2nose=Y3nose
5030    GOTO 5060
5040    Y2nose=Aa+Bb*Xprime
5041    Y3nose=B(7,1)+B(7,2)*X2nose
5042    IF Y3nose<=Y2nose THEN Y2nose=Y3nose
```

TRAJECTORY WITH ICE ABLATION

```
5048  ! ***************************************************************
5049  !
5050  ! IF NOSE SHAPE IS TO BE PRINTED A STATEMENT HERE SHOULD BE:"IF TOTIME=INT
      (TOTIME) THEN PRINT .2,XZERO,XPRIME,Y2NOSE" AND CHANGE LINE 5030 TO "GO TO 5050
5060     Dr=Y2nose-Ynose
5070     Dx=X2nose-Xnose
5080     Theta=ATN(Dr/Dx)
5090     Cp=Cpo*SIN(Theta)^2
5100     Drag=PI*Q*Cp*(Y2nose^2-Ynose^2)/144
5110     Total_drag=Total_drag+Drag
5120     Volume=((Y2nose+Ynose)/2)^2*PI*Dx+Volume
5130     IF X2nose=60 THEN 6000
5140     Xnose=X2nose
5150     Ynose=Y2nose
5151     IF Xprime>2.4 THEN F=5
5160     GOTO 5003
6000     IF L>0 THEN 6013
6001     Tvolume=Volume
6002     Tmass=1.4*Tvolume*62.4/(32.2*12^3)
6003     L=L+1
6004     Base_area=PI*Y2nose^2
6005     PRINT
6006     PRINT "INITIAL VOLUME=",Tvolume,"CUBIC INCHES"
6007     PRINT "INITIAL MASS=",Tmass,"SLUGS"
6008     PRINT "BASE AREA=",Base_area,"SQUARE INCHES"
6009     PRINT
6010     PRINT
```

97

TRAJECTORY WITH ICE ABLATION

```
6011   PRINT "TIME","ALTITUDE","RANGE","VOLUME"
6012   PRINT "TOTAL DRAG","MACH NO","Cd","BETA"
6013   IF Tvolume-Volume<0 THEN Volume=Tvolume
6014   Dmass=Rhomissile*(Tvolume-Volume)
6015   IF Z=2 THEN 6017
6016   IF Y2<=Cloud_altitude THEN 8000
6017   Cd=Total_drag/(Q*Base_area/144)
6018   Beta=(Tmass-Dmass)*G/(Cd*Base_area/144)
6019   PRINT
6020   PRINT Totime,Y2,X2,Volume,Total_drag,Mach_no,Cd,Beta
6021   PRINT
6030   IF K=1 THEN 7000
6040   GOTO 2000
7000   PRINT "IMPACT RANGE IS",X2/6076.12,"NAUTICAL MILES"
7001   PRINT "CLOUD PARAMETERS ARE:"
7002   PRINT "MASS LOSS FACTOR = ",Mass_factor
7003   PRINT "CLOUD ALTITUDE = ",Cloud_altitude,"FEET"
7004   PRINT "CLOUD THICKNESS = ",Cloud_thickness,"FEET"
7005   PRINT "CLOUD DENSITY = ",Cloud_density*454*32.2/.3048^3,"G/M3"
7006   PRINT "MASS LOSS DUE TO ICE IMPACT = ",Mass_loss,"SLUGS"
7007   PRINT "VOLUME LOSS DUE TO ICE IMPACT = ",Volume_loss,"CU IN"
7008   PRINT "EQUIVALENT ALTITUDE CHANGE DUE TO ICE CLOUD = ",Delta_h,"FEET"
7009   STOP
7010   END
7910   ! *************************************************
7911   ! THE FOLLOWING SECTION CALCULATES THE MASS LOSS DUE TO ICE ABLATION. IT
       ALSO CHANGES THE NOSE SHAPE TO ACCOUNT FOR THIS MASS LOSS.
7912   !
```

TRAJECTORY WITH ICE ABLATION

```
8000    IF Z=1 THEN 8500
8010    Swept_volume=Base_area*Cloud_thickness/(ABS(SIN(Ainitial))*144)
8020    Mass_loss=Mass_factor*Cloud_density*Swept_volume
8030    Volume_loss=Mass_loss/Rhomissile
8040    Mass_ablated=Dmass+Mass_loss
8050    Delta_h1=0
8060    Delta_h=-1000
8070    Dmass1=Dmass
8080    Z=1
8090    GOTO 2105
8500    Delta_h2=Delta_h
8510    IF ABS(Mass_ablated-Dmass)<.001 THEN Z=2
8520    IF Z=2 THEN 6017
8530    Delta_h=Delta_h-(Delta_h1-Delta_h)*(Mass_ablated-Dmass)/(Dmass-Dmass1)
8540    Delta_h1=Delta_h2
8550    Dmass1=Dmass
8600    GOTO 2105
8910    ! *************************************************************
8911    ! THE FOLLOWING SECTION CALCULATES THE FINAL RANGE USING LINEAR INTERPO-
        LATION BETWEEN THE LAST POINT ABOVE THE GROUND AND THE FIRST POINT BELOW
8912    !
9000    Xrange=(X2*Y3-X3*Y2)/(Y3-Y2)
9010    V=(0-Y2)/(Dtime*(Xrange-X2)/(X3-X2))
9020    U=(Xrange-X2)/(Dtime*(Xrange-X2)/(X3-X2))
9030    X2=Xrange
9040    Y2=0
9050    K=1
9060    GOTO 4000
```

99

LIST OF REFERENCES

1. Air Force Cambridge Research Laboratories Report 73-0423, An Assessment of the Carbon Humidity Element in Radiosonde Systems by Frederick J. Brousaides, 18 July 1973.

2. Loh, W. H. T., Dynamics and Thermodynamics of Planetary Entry, Prentice-Hall, 1963.

3. Fuhs, A. E., "Ballistic Missile Notes," AE 4705, Naval Postgraduate School, 1980.

4. Cox, R. N. and Crabtree, L. F., Elements of Hypersonic Aerodynamics, Academic Press, 1965.

5. Lees, L., "Hypersonic Flow," Proceedings of the Fifth International Aeronautical Conference in Los Angeles, Institute of Aeronautical Sciences, p. 241-276, 1955.

6. North Atlantic Treaty Organization Advisory Group for Aerospace Research and Development, AGARDograph No. 161, Ablation, by H. Hurwicz, K. M. Kratsch, and J. E. Rogan, Technical Editing and Reproduction, March 1972.

7. Loh, W. H. T., Reentry and Planetary Entry Physics and Technology, Vols. I and II, Springer-Verlag, 1968.

8. Heymsfield, A., "Cirrus Uncinus Generating Cells and the Evolution of Cirroform Clouds. Part 1: Aircraft Observations of the Growth of the Ice Phase," Journal of the Atmospheric Sciences, Vol. 32, No. 4, pp. 799-808, April 1975.

INITIAL DISTRIBUTION LIST

No. Copies

1. Defense Technical Information Center   2
   Cameron Station
   Alexandria, Virginia 22314

2. Library, Code 0142   2
   Naval Postgraduate School
   Monterey, California 93940

3. Department Chairman, Code 69   1
   Department of Mechanical Engineering
   Naval Postgraduate School
   Monterey, California 93940

4. Distinguished Professor A. E. Fuhs, Code 67   3
   Department of Aeronautics
   Naval Postgraduate School
   Monterey, California 93940

5. RADM Glenwood Clark, Jr., Code NSP-20   1
   Technical Director
   Strategic Systems Project Office
   Department of the Navy
   Washington, D.C. 20376

6. CDR H. S. Nakayama, Code NSP-272   1
   Strategic Systems Project Office
   Department of the Navy
   Washington, D.C. 20376

7. LCDR Robert W. Stevenson   1
   Strategic Systems Project Office
   Department of the Navy
   Washington, D.C. 20376

8. Mr. Allen Sumida   1
   Naval Plant Representative Office
   Sunnyvale, California 94088

9. LCDR Martin Warren Mellor, USN   3
   139 Grand Avenue
   Wood River, Illinois 62095